ACS OMEGA

Open Access

http://pubs.acs.org/journal/acsodf

Article

Bilayered Film Modified Glassy Carbon Electrode for the Simultaneous Determination of Paracetamol and Chloroquine in Pharmaceutical and Biological Samples

Mulu Gashu,* Belete Asefa Aragaw,* Molla Tefera,* and Atakilt Abebe

Cite This: *ACS Omega* 2025, 10, 5601−5615

Read Online

ACCESS | Metrics & More | Article Recommendations | Supporting Information

ABSTRACT: A new, cost-effective selective and highly sensitive electrochemical sensor (poly(cobalt(II) bis(1,10-phenanthroline) and copper(I) bis(2,2-bipyridine)), poly(Co(Phen)$_2$/Cu(Bip)$_2$)/GCE) was synthesized based on the sequential electropolymerization of diaquabis(1,10-phenanthroline) cobalt(II)-iodide dehydrate ([Co(Phen)$_2$(H$_2$O)$_2$]I$_2$·2H$_2$O) and bis(2,2′-bipyridine)hydroxyl copper(II) iodide ([Cu(Bip)$_2$OH]I) at a glassy carbon electrode. The established sensor (poly(Co(Phen)$_2$/Cu(Bip)$_2$)/GCE)) was employed for the simultaneous electrochemical determination of paracetamol (PCM) and chloroquine (CQ). The established sensor was characterized by FTIR, cyclic voltammetry (CV), and electrochemical impedance spectroscopy (EIS). The electrochemical performance of unmodified GCE and poly(Co(Phen)$_2$/Cu(Bip)$_2$)/GCE was evaluated for the simultaneous voltammetric determination of PCM and CQ. Using poly(Co(Phen)$_2$/Cu(Bip)$_2$)/GCE and optimized conditions, the simultaneous square wave voltammetric determination of PCM and CQ shows linearity in the concentration range between 0.5 and 200 μM, with sensitivity of 0.389 and 0.462 μA/μM and detection limits (LOD) of (3δ/m) 4.38 × 10^{-2} and 7.48 × 10^{-2} μM, respectively. Poly(Co(Phen)$_2$/Cu(Bip)$_2$)/GCE showed excellent performance for the simultaneous sensing of PCM and CQ in pharmaceutical, serum, and urine samples, with spiked recoveries exceeding 98.9, 97.9, and 98.2%, respectively, demonstrating low LOD, excellent sensitivity, admirable selectivity, venerable repeatability, and long-lasting stability. Poly(Co(Phen)$_2$/Cu(Bip)$_2$)/GCE's selectivity for the simultaneous determination of PCM and CQ was shown, demonstrating excellent selectivity despite potential interferences like sulfamethoxazole (SMX), salbutamol (SBM), guanine (Gua), and atorvastatin (ATS). These results designate that poly(Co(Phen)$_2$/Cu(Bip)$_2$)/GCE exhibits admirable applicability for the simultaneous electrochemical sensing of PCM and CQ in various real samples.

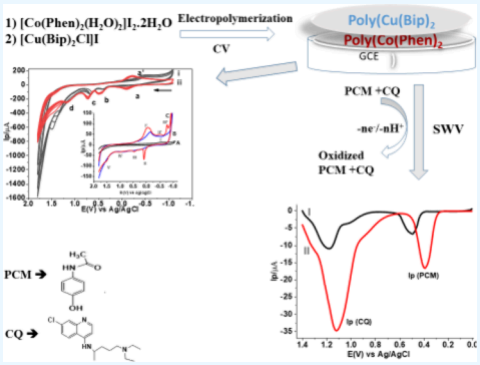

1. INTRODUCTION

N-Acetyl-*p*-aminophenol, or PCM, is another name for acetaminophen, which is commonly used as an analgesic and antipyretic drug. It has also been the main active component in pharmaceutical formulations with many components and is frequently used to treat disorders connected to headaches and other conditions affecting various body regions.[1] To treat minor discomfort and fever, PCM is usually used in conjunction with antibiotics like levofloxacin, amoxicillin, ciprofloxacin, chloroquine, and others.[2,3] The maximum recommended dosage of paracetamol has been documented at dosages below 40 mg/kg.[4] In therapeutic dosages, this medicine is safe to use; nevertheless, if used in more than recommended amounts, it can act as a hepatotoxic and cause substantial harm to the liver, as well as possibly other organs.[5,6]

Chloroquine (CQ, N4-(7-chloro-4-quinolinyl)-N1,N1-diethylpentane-1,4-diamine diphosphate) is an antibiotic belonging to the quinolone family that is useful in treating respiratory infections, urinary tract infections, gastrointestinal disorders, malaria, and systemic lupus erythematosus.[7,8] However, if this treatment is used excessively, it may lead to the creation of additional antibiotic-resistant bacteria and health issues.[9−11] When used as directed and in the administered quantity, CQ is usually regarded as a safe medication for several illnesses. The aged-based total dose of chloroquine is expressed in milligrams of medicine per kilogram of body weight (mg/kg). An acceptable therapeutic efficacy of chloroquine has been documented at dosages below 25 mg/kg.[12,13]

Published findings state that persons with bacterial infections usually experience fever and/or inflammation. Antibiotics should be utilized in combination with nonantibiotic drugs to treat these symptoms.[3] Moreover, studies carried out both in vitro and in vivo have demonstrated a

Received: September 18, 2024
Revised: January 18, 2025
Accepted: January 27, 2025
Published: February 5, 2025

synergistic impact when antibiotics and antipyretics are administered together.[14] Thus, combining nonantibiotic drugs with antibiotics compromises a chance to investigate a formerly uncharted area of the bioactive chemical space. Antipyretic drugs are therefore recommended to be used in combination with antibiotics in medical treatments.[14,15] Antipyretic and antibiotic drugs are not usually obtainable together in pharmaceutical medications, although they are occasionally utilized in treatments. However, certain antipyretic formulations also have antihistaminic and antiallergic qualities. Nonetheless, considering the synergy that arises from mixing antipyretic and antibiotic formulations, it is crucial to develop an analytical method that is sensitive, selective, and economical for determining these agents simultaneously to determine their concentration in biological fluids and pharmaceutical formulations.[14]

Analytical techniques like colorimetry and refractometry methods[16] and HPLC[17] have been utilized for the simultaneous sensing of CQ and PCM in pharmaceutical and biological samples.[18] Compared with the previously described approaches, electroanalytical techniques provide the potential benefits of low cost, short analysis times, and high sensitivity. Meanwhile, because of their high overpotential, low selectivity, sluggish kinetics, poor sensitivity, and overlapping electrochemical signals, conventional electrodes' electrochemical response for simultaneous voltammetric measurement of analytes is rather limited.[19−21]

Consequently, limited studies utilizing chemically modified electrodes, such as nickel oxide nanoparticles modified glassy carbon electrode (NiONPs/GCE),[3] copper zinc ferrite nanoparticles modified carbon paste electrode (CZF-CPE),[14] a binary layer of poly(1,5-diaminonaphthalene) and platinum nanoparticles (PtNPs/p-1,5-DAN/Pt electrode),[22] boron-doped diamond electrode,[23] 3D printed disposable electrode,[24] platelet-like strontium vanadate (SrV) supported on a graphitic carbon nitride (SrV/GCN) nanocomposite modified electrode (SrV/GCN/GCE),[25] and *N*,*N*-bis[(*E*)-(1-pyridyl)-methylidene]-1,3-propanediamine (PMPDA) self-assembled monolayer (SAM) modified electrode (PMPDA SAM/GCE,)[26] have been published for the simultaneous electroanalytical detection of antibiotic and antipyretic drugs in pharmaceutical and biological samples.

Because of their catalytic ability to lower the overpotential of the targeted electroactive analyte employed in electroanalytical results, conducting polymers based on transition metal complexes have garnered a great deal of attention in the field of electrode modification these days.[27] Numerous techniques, including the self-assembling method,[28,29] adsorption,[30] and electropolymerization,[31] have been used to produce modified electrode surfaces based on metal complexes.

A transition metal complex is a chemical species comprising a central atom or ion, which is typically metallic and is called the *coordination center*, and a neighboring arrangement of bound molecules or ions that are in turn known as ligands or complexing agents. Transition metal complexes are widely recognized compounds with numerous uses in analytical, antibacterial, anticarcinogenic, and medicinal applications.[32] In recent years, metal complexes have been used in the electrode modification process, which serve as quick electron transfer mediators in the electrochemical reaction by lowering the overpotential of the electroactive substance.[33] This could be achieved by carefully designing and synthesizing transition metal coordination complexes from carefully identified and selected transition metal ions with appropriate ligands so that they would have polymerizable electroactivity, a geometry that results in a porous and large surface area over the electrode surface and, consequently, high charge movements in the entire polymer with appropriate redox potentials so that it could oxidize or reduce the analytes in given samples. For this purpose, certain transition metal ion complexes could be good candidates and have been the focus of study. Several reports indicate their promising efficient performances.[34−37] Based on this, copper(II) and cobalt(II) with ligands such as 2,2′-bipyridine(Bip) and 1,10-phenanthroline(Phen) are identified as perfect couples that result in complexes that undertake redox activities by switching between its +2 and +1, and +2 and +3 oxidation states, respectively, in desirable potential ranges in which the selected analyte is investigated with greater sensitivity and enhanced selectivity when an electroactive species is oxidized (reduced) slowly at the conventional electrode at a higher magnitude of the redox potential.[38] Bip is a colorless heteroaromatic solid and an important isomer of the bipyridine family. Phen is a tricyclic rigid heteroaromatic molecule. Both form chelate complexes with most d-block metals through both σ-donating nitrogen atoms and π-accepting properties.[39−42]

Besides their effective electron transfer activity and catalytic activity, transition metal complexes can be electropolymerized layer by layer to immobilize two-layered conducting polymeric films onto the electrode surface.[20] The bilayered (hybrid) films offer a synergistic framework with a distinctive combination of properties, enhanced electrical conductivity, and large surface area.[43,44] The bilayered films enhance the electrochemical performance of the sensor depending on the sensitivity, detection limit, selectivity, multifunctionality, and miniaturization.[45]

To the best of our knowledge, no reports have been made for the simultaneous voltammetric sensing of PCM and CQ using bilayered films of electropolymerized cobalt and copper complex modified glassy carbon electrode (poly($Co(Phen)_2$/$Cu(Bip)_2$)/GCE). Accordingly, for the simultaneous voltammetric measurement of PCM and CQ in pharmaceuticals and biological samples, a sensitive and economical voltammetric approach based on poly($Co(Phen)_2$/$Cu(Bip)_2$)/GCE was suggested.

2. MATERIALS AND METHODS

2.1. Chemicals and Reagents. The following analytical-grade chemicals and reagents were utilized without further purification: paracetamol (PCM, 99.8%, Merck), chloroquine phosphate (99%, Sigma-Aldrich), dihydrated copper chloride ($CuCl_2{\cdot}2H_2O$), sulfuric acid (98% Loba Chemie, laboratory reagent), methanol (>99.0%, BDH Laboratories Supplies, England), $CoCl_2{\cdot}6H_2O$, potassium iodide (KI) (99.5%, Blulux Laboratories (p) Ltd.), potassium hexacyanoferrate (II), sodium dihydrogen phosphate (NaH_2PO_4), 1,10-phenanthroline monohydrate (BDH Chemical Ltd., Poole, England), sodium hydroxide (extra pure, LabTech Chemicals), 2,2′-bipyridine (99.7%, Sigma-Aldrich), potassium hexacyanoferrate (III) (98.0%, BDH Laboratories Supplies, England), sodium monohydrogen phosphate (Na_2HPO_4) (98%, Blulux Laboratories (p) Ltd.), and hydrochloric acid (37%, Fisher Scientific).

2.2. Instrumentation. Using a CHI 760E potentiostat workstation (Austin, TX, USA), the voltammetric measurement was performed. Three electrodes made up the electro-

https://doi.org/10.1021/acsomega.4c08563
ACS Omega 2025, 10, 5601−5615

chemical cell: a saturated silver/silver chloride (Ag/AgCl) electrode, a modified and unmodified glassy carbon electrode composed of poly($Co(Phen)_2$)/$Cu(Bip)_2$, and a platinum coil (Pt) that served as the reference, working, and counter electrodes, respectively. The DR6000 UV VIS Spectrophotometer, an atomic absorption spectrophotometer (Analytik Jena Nov AA300), an electronic balance (Nimbus, Adam Equipment, USA), the Avatar 330 FTIR Thermo Nicolet spectrophotometer, a deionizer (Evoqua Water Technologies, Germany), a conductivity meter (Jenway 4200), a pH meter (AD8000, Adwa, Romania), and a melting point apparatus (Stone, Staffordshire, ST15 OSA, UK) were among the apparatus and equipment used in the experiment.

2.3. Poly($Co(Phen)_2$)/$Cu(Bip)_2$)/GCE Preparation. The synthesis procedure of $[Cu(Bip)_2Cl]I$ and $[Co(Phen)_2(H_2O)_2]I_2{\cdot}2H_2O$ complexes was described in our previous works.[46,47] The bare GCE was meticulously polished using alumina powder (0.05, 0.3, and 1 μm) before synthesizing poly($Co(Phen)_2$)/($Cu(Bip)_2$)/GCE. The leftover polishing powder was then repeatedly removed by washing the GCE using distilled water. Next, 2 mM $[Co(Phen)_2(H_2O)_2]I_2{\cdot}2H_2O$ was electropolymerized to form the poly($Co(Phen)_2$) coating on the polished and air-dried GCE surface in 0.1 M of PBS of pH 7 by cyclic voltammetry ranging between -1.1 and +1.8 V at 50 mV/s for 10 cycles. After carefully rinsing the resulting poly($Co(Phen)_2$)/GCE with distilled water, it was scanned in a monomer-free 0.5 M H_2SO_4 between −1.1 and +1.8 V until a steady-state cyclic voltammogram appeared. Using 2 mM of $[Cu(Bip)_2Cl]$, the same process was used to prepare poly($Cu(Bip)_2$)/GCE. The bilayered film-modified GCE poly($Co(Phen)_2$)/$Cu(Bip)_2$)/GCE was then produced by varying the number of polymerization scan cycles of 2 mM $[Co(Phen)_2(H_2O)_2]I_2{\cdot}2H_2O$ and 2 mM $[Cu(Bip)_2Cl]I$. The first poly($Co(Phen)_2$/$Cu(Bip)_2$)/GCE was prepared through electropolymerization of 2 mM $[Co(Phen)_2(H_2O)_2]I_2{\cdot}2H_2O$ at the GCE surface for 10 scan cycles without electropolymerization of 2 mM $[Cu(Bip)_2Cl]I$. Then, the poly($Co(Phen)_2$/$Cu(Bip)_2$)/GCE was prepared via electropolymerization of eight scan cycles of $[Co(Phen)_2(H_2O)_2]I_2{\cdot}2H_2O$ and two scan cycles of $[Cu(Bip)_2Cl]I$ at the GCE surface. The same electropolymerization procedure was also carried out for 6:4, 4:6, and 2:8 scan cycle ratios of $[Co(Phen)_2(H_2O)_2]I_2{\cdot}2H_2O$ and $[Cu(Bip)_2Cl]I$, respectively, at the GCE surface. A similar sequential electropolymerization procedure was conducted for 10:0, 8:2, 6:4, and 4:6, 2:8 scan cycle ratios of 2 mM $[Co(Phen)_2(H_2O)_2]I_2{\cdot}2H_2O$ and $[Cu(Bip)_2Cl]I$, respectively, to synthesize poly($Cu(Bip)_2$/$Co(Phen)_2$)/GCE. Then, the prepared poly($Co(Phen)_2$/$Cu(Bip)_2$)/GCE and poly($Cu(Bip)_2$/$Co(Phen)_2$)/GCE were cleaned using distilled water to remove loosely adsorbed monomer particles on GCE. Finally, the prepared electrode was dried in air and used for additional tests after being stabilized for 2 min in a monomer-free 0.5 M H_2SO_4 until a stabilized CV was seen.

2.4. Solution Preparations. To prepare a 5.0 mM solution of PCM and CQ, 38 and 80 mg of the CQ and PCM standard, respectively, were dissolved in a 50 mL volumetric flask using deionized water. The 5.0 mM of PCM and CQ standard was diluted using 0.1 M PBS that was made from an equimolar concentration of NaH_2PO_4 and Na_2HPO_4 to prepare the working solutions of PCM and CQ.

To do real sample analysis, two brands of PCM and CQ tablets (ASKON, India, and EPHARM, Ethiopia) were purchased from a local pharmacy in Bahir Dar, Ethiopia. According to the manufacturer's license, the nominal values of PCM and CQ were 500 and 250 mg/tablet, respectively, as electroactive ingredients. Using a pestle and mortar, five tablets were completely ground and blended into a suitable powder. Although the two brands (ASKON and EPHARM) of PCM consist of 500 mg/tablet active ingredients, due to the presence of inactive ingredients, the average weight mass was 638.8, and 555.96 mg/tablet, respectively. Similarly, the typical measured mass of the CQ tablet sample was 387.6 and 297.72 mg/tablet for ASKON and EPHARM, respectively. Deionized water was used to dissolve 48.6 and 124.04 mg and 42.2 and 95.3 mg of PCM and CQ of EPARM and ASKON tablet powder, respectively, into a 50 mL volumetric flask to create stock solutions (5.0 mM) of the tablet samples. The PCM and CQ sample solutions were diluted in PBS at pH 6 to get the final concentrations within the calibration curve's linear range.

Serum and urine samples were acquired at the Tibebe Ghion referral hospital located in Bahir Dar, Ethiopia. After that, the serum (0.5 mL) was put into a volumetric flask (25 mL), and pH 6 of 0.1 M PBS was added up to the mark. The same procedure was used for urine sample solution preparation. To do a recovery analysis, the urine sample solution and serum were also made in a 25 mL flask with a 0.5 mL urine sample using PBS. Finally, 25 and 50 μM PCM and CQ standard solution were spiked into the urine sample solution for recovery analysis. When it was not in use, the prepared sample solution was stored in the refrigerator and used for the electrochemical measurement.

3. RESULTS AND DISCUSSION

3.1. Fabrication of Poly($Co(Phen)_2$/$Cu(Bip)_2$)/GCE. The poly($Co(Phen)_2$/$Cu(Bip)_2$)/GCE was produced using the method mentioned in Section 2.3. $[Co(Phen)_2(H_2O)_2]I_2{\cdot}2H_2O$ and $Cu[(Bip)_2Cl]I$ were electropolymerized in the range of −1.1 to +1.8 V for 10 cycles at a scan rate of 100 mV/s. The electropolymerization of 2 mM of $[Co(Phen)_2(H_2O)_2]I_2{\cdot}2H_2O$ (i) and $[Cu(Bip)_2Cl]I$ (ii) and the steady-state stabilization of the poly($Co(Phen)_2$/$Cu(Bip)_2$)/GCE by monomer-free 0.5 M H_2SO_4 in −1.1 and +1.8 V potential range are depicted in Figure 1i,ii (inset of Figure 1). The identified redox peaks in the electropolymerization CVs of $[Co(Phen)_2(H_2O)_2]I_2{\cdot}2H_2O$ (i) and $[Cu(Bip)_2Cl]I$ (ii) at the GCE surface verify the presence of the electroactive functional groups in the monomer species.[46,47] Different sequential electropolymerization scan cycle ratios of $[Co(Phen)_2(H_2O)_2]I_2{\cdot}2H_2O$ and $[Cu(Bip)_2]Cl$ ($[Co(Phen)_2(H_2O)_2]I_2{\cdot}2H_2O$/$[Cu(Bip)_2]Cl$)—10:0, 8:2, 6:4, 4:6, 2:8, and 0:10—were used to make the bilayer electropolymerized films of ($Co(Phen)_2$/$Cu(Bip)_2$) ($Co(Phen)_2$/$Cu(Bip)_2$). The $Cu(Bip)_2$/$Co(Phen)_2$ polymeric films were also prepared by varying the sequence of the electropolymerization of the two monomers ($[Cu(Bip)_2Cl]$ and $[Co(Phen)_2(H_2O)_2]I_2{\cdot}2H_2O$) at the GCE surface. Figure 1 depicts the voltammetric response of the sequential electropolymerization of 2 mM $[Co(Phen)_2(H_2O)_2]I_2{\cdot}2H_2O$ and $[Cu(Bip)_2Cl]I$ in the PBS of neutral pH on GCE in the potential window of −1.1 and 1.8 V for four (i) and six (ii) scan cycles. The presence of different redox peaks (*a*, *b*, *c*, *d*, and *a*′ and *w*, *x*, *y*, *z*, *x*′, and *w*′) in the CVs of $[Cu(Bip)_2Cl]$ and $[Co(Phen)_2(H_2O)_2]I_2{\cdot}2H_2O$, respectively, indicates the appearance of a large number of electroactive functional groups in the monomers. As displayed in the inset of Figure 1, the formation of six new peaks in curve C (two reductive: II′

https://doi.org/10.1021/acsomega.4c08563
ACS Omega 2025, 10, 5601−5615

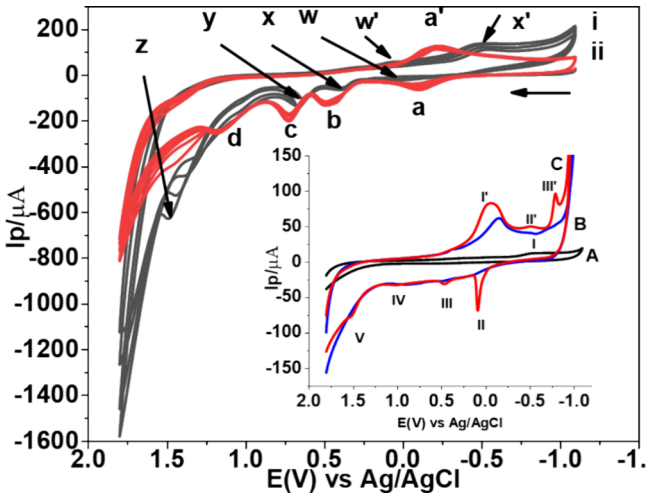

Figure 1. CVs of the sequential electropolymerization of 2 mM $[Co(Phen)_2(H_2O)_2]I_2{\cdot}2H_2O$ and $[Cu(Bip)_2Cl]I$ in 0.1 M PBS of pH 7 on GCE in the range between −1.1 and 1.8 V for four and six scan cycles, respectively, at 50 mV/s of scan rate. Inset: CVs of (A) GCE, (B) poly$(Co(Phen)_2)$/GCE, and poly$(Co(Phen)_2/Cu(Bip)_2)$/GCE in 0.5 M H_2SO_4 stabilized in the potential range between −1.1 and +1.8 V at 100 mV/s.

and III' and four oxidative: II, III, IV, and V) that were not visible at GCE (curve A) validates the successful fabrication of modified GCE.

The electropolymerization mechanism of monolayer $Co(Phen)_2(H_2O)_2]I_2{\cdot}2H_2O$ and $[Cu(Bip)_2Cl]I$ at GCE was described in our previous works.[46,47] The proposed polymerization of the mechanism of the synthesized bilayered film at the GCE surface is clarified in Scheme 1. During the electropolymerization process, the oxidation of the top layer (poly$(Cu(Bip)_2)$ cannot take place until the reaction process produces enough charge carriers for the oxidation of the bottom layer (poly$(Co(Phen)_2)$. As a result, the poly$(Co(Phen)_2)$ layer helps as a redox mediator for the movement of electrons from the electrode surface to poly$(Cu(Bip)_2)$, and its ongoing regeneration results in a notable rise in the faradaic current when interrelated to the poly$(Co(Phen)_2)$ layer alone.[48]

The simultaneous electrochemical oxidation of PCM and CQ was examined by measuring the CV response of each modified electrode that was fabricated at a varied ratio of the two monomers. In poly$(Co(Phen)_2/Cu(Bip)_2)$/GCE, which was synthesized in varying ratios of monomer scan cycles, the simultaneous electrochemical response of 1 mM PCM and CQ at poly$(Co(Phen)_2/Cu(Bip)_2)$/GCE and poly$(Cu(Bip)_2/Co$-

Scheme 1. Proposed Sequential Electropolymerization Mechanism of $[Co(Phen)_2(H_2O)_2]I_2{\cdot}2H_2O$ and $[Cu(Bip)_2Cl)$ at a Glassy Carbon Electrode

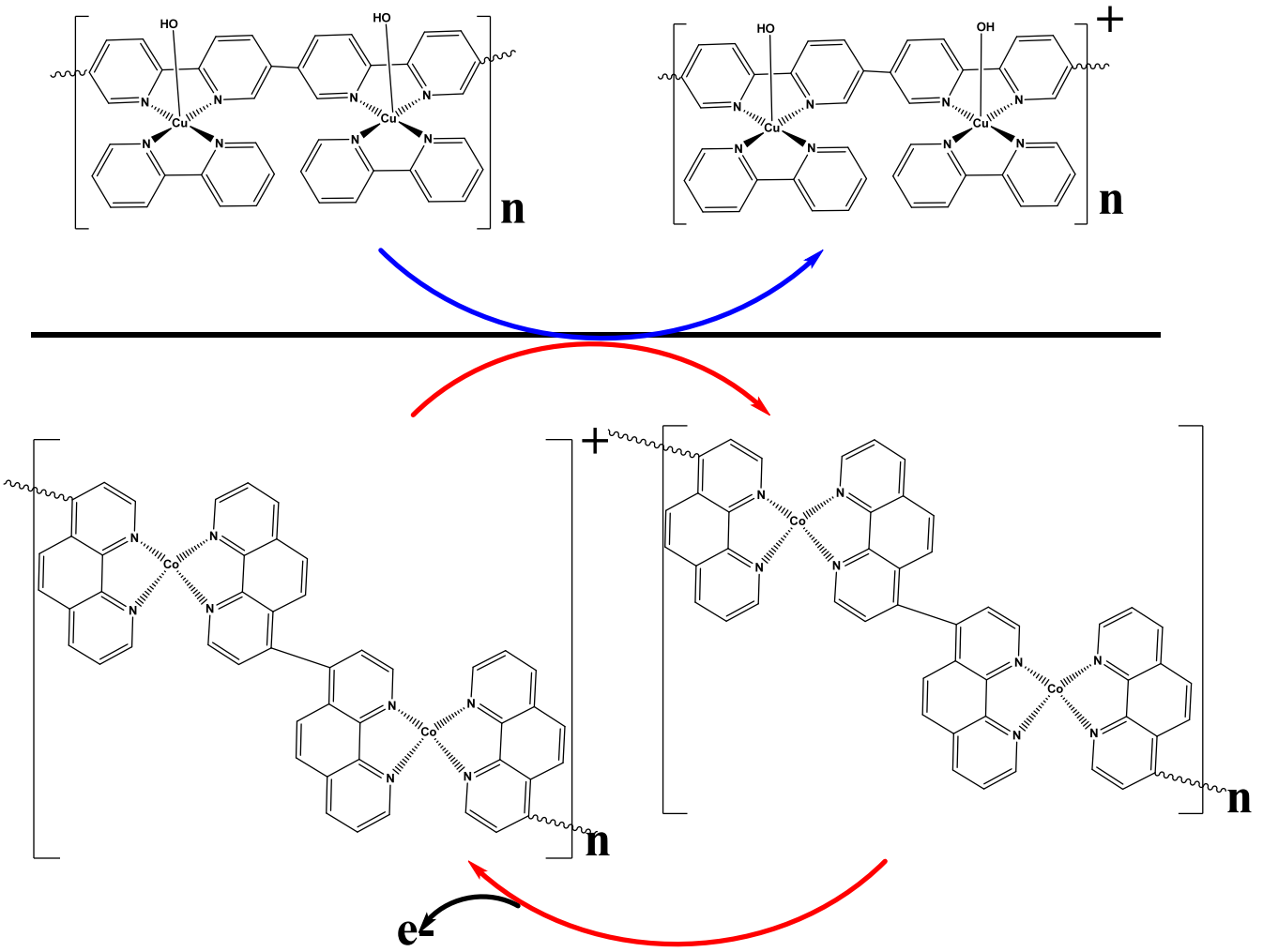

https://doi.org/10.1021/acsomega.4c08563
ACS Omega 2025, 10, 5601−5615

$(Phen)_2$)/GCE is shown in Figure 2A,B. The simultaneous voltammetric response of PCM and CQ at poly(Co$(Phen)_2$/

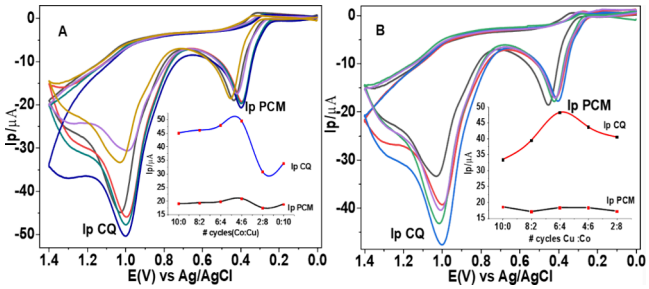

Figure 2. CVs of 1 mM PCM and CQ in 0.1 M PBS of pH 7.0 at (A) poly(Co$(Phen)_2$/Cu$(Bip)_2$)/GCE prepared from 10:0, 8:2, 6:4, 4:6, 2:8, and 0:10 ratio of $[Co(Phen)_2(H_2O_2)]I_2{\cdot}2H_2O$ and [Cu$(Bip)_2Cl]I$, respectively. and (B) poly(Cu$(Bip)_2$/Co$(Phen)_2$)/GCE prepared from 10:0, 8:2, 6:4, 4:6, 2:8, and 0:10 ratio of [Cu$(Bip)_2Cl]I$ and $[Co(Phen)_2(H_2O_2)]I_2{\cdot}2H_2O$, respectively. Inset: plot of the peak current of PCM and CQ against the ratio of polymerization scan cycles of $[Co(Phen)_2(H_2O_2)]I_2{\cdot}2H_2O$ and [Cu$(Bip)_2Cl]I$.

Cu$(Bip)_2$)/GCE shows better peak current enhancement as compared to poly(Cu$(Bip)_2$/Co$(Phen)_2$)/GCE. Moreover, as revealed in the inset of Figure 2A, the poly(Co$(Phen)_2$/Cu$(Bip)_2$)/GCE prepared at a 4:6 ratio of $[Co(Phen)_2(H_2O)_2]I_2{\cdot}2H_2O$ and [Cu$(Bip)_2Cl]I$ electropolymerization cycles demonstrates superior peak current enhancement compared to the other electrodes. As a result, the bilayered film that was synthesized via a 4:6 scan cycles ratio of the two complexes ($[Co(Phen)_2(H_2O)_2]I_2{\cdot}2$ H_2O/[Cu$(Bip)_2Cl]I$) was preferred as the optimum bilayered film thickness for further experiments.

3.2. Characterization of Poly(Co$(Phen)_2$/Cu$(Bip)_2$)/GCE. *3.3.1. FTIR.* FTIR analysis could provide insights into the structural changes and interactions occurring in the complexes involved during the electropolymerization process, highlighting the bond order and strength changes within the complexes, evidenced by the presumable characteristic vibrational frequency changes. The coordinated water and crystallization of water in $[Co((Phen)_2(H_2O)_2]I_2{\cdot}2H_2O$ were eliminated in the polymerization procedure, as shown by the infrared spectrum of the electropolymerized product. The nonappearance of the characteristic bands in the [Co-$((Phen)_2(H_2O)_2]I_2{\cdot}2H_2O$ spectra, which are situated at 3495 and 3345 cm^{-1}, serves as evidence for this (Figure 3A).[47]

The broad signal observed between 3229 and 3177 cm^{-1} in the FTIR spectrum of the composite (Figure 3C) resembles the νO−H bonds present in the hydroxide group that are coordinated to [Cu(bip)$_2$Cl]I, where the chloride ion has been replaced by the hydroxide ion, leading to the formation of [Cu$(bip)_2(OH)]I$ that was signaled at 3441 cm^{-1} (Figure 3B) during the polymerization process. The broadness of this band is attributed to the interactions of the hydroxide group with various hydrogen atoms from the coordinated 2,2′-bipyridine ligands.[46] The types and proximities of these hydrogen atoms influence this interaction. Moreover, the hydroxides on the surface and the bilayer interface created different electronic environments and contributed to the band's broadness. The bands observed at 1461 and 1368 cm^{-1} are allocated to νC−C and C−N, respectively, of both phen and bip (Figure 3C).

Additionally, a distinctive peak observed at 2962 cm^{-1} can be assigned to νC−H bonds within the fused ring structure of the phenanthroline moiety in complex $[Co(phen)_2(H_2O)_2]I_2$. Another prominent peak at 2853 cm^{-1} is associated with the νC−H originating from the N═C−H groups present in the phenanthroline and bipyridine ligands of the complexes, whose bond order is significantly decreased following the electropolymerization. Furthermore, the absorption band at 2926 cm^{-1} resembles the νC−H bonds within the C═C−H groups from phen and bip (Figure 3C,D) whose bond order is decreased in the same manner as N═C−H. Furthermore, the

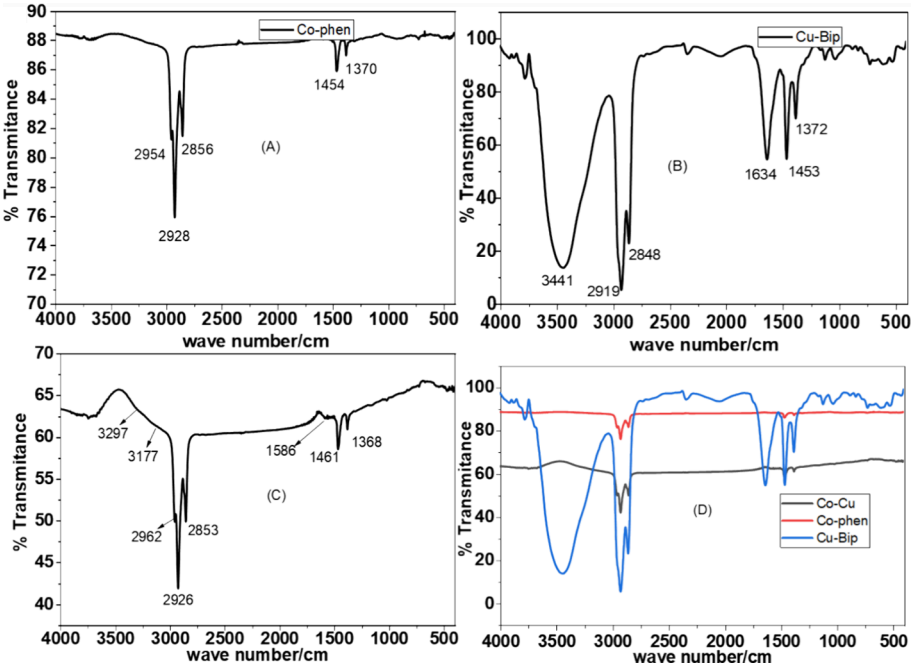

Figure 3. FTIR spectra of (A) poly(Co$(phen)_2$), (B) poly(Cu$(bip)_2$), and (C) poly(Co$(phen)_2$)/poly(Cu$(bip)_2$) composite (bilayer). (D) Overlay of panels A, B, and C.

https://doi.org/10.1021/acsomega.4c08563
ACS Omega 2025, 10, 5601−5615

strong band at 1634 cm^{-1} in the spectrum of poly[Cu(bip)Cl]I (Figure 3B) characteristic of $\nu C{=}C$ is found to change to 1586 cm^{-1} in the spectrum of the bilayered composite (Figure 3D).

In the FTIR spectra comparison between poly$(Co(Phen)_2)$ (Figure 3A) and poly$(Cu(Bip)_2)$ (Figure 3B), it is noted that poly(Co(Phen)2) exhibits a lower number of peaks compared to poly$(Cu(Bip)_2)$. This discrepancy is attributed to structural differences: poly$(Co(Phen)_2)$ features a tricyclic rigid structure that efficiently cancels out net dipole moments, leading to the absence of certain peaks. Instead, poly$(Cu(Bip)_2)$ comprises a bicyclic nonrigid molecule, allowing for more freedom of motion and fewer dipole moment cancellations, thus resulting in the presence of multiple peaks.

When analyzing the bilayer spectrum (Figure 3C), a reduced number of peaks is observed. This reduction is hypothesized to stem from limitations on the motion freedom of the bipyridine rings due to $\pi{-}\pi$ interactions with the 1,10-phenanthroline moiety in the adjacent layer. These interactions enhance dipole cancellation, consequently diminishing the appearance of distinct peaks in the spectrum.

Taken together, these spectral features suggest the formation of a bilayer polymer structure involving the two complexes under investigation.

3.3.2. Cyclic Voltammetry. The performance of the bare GCE, poly$(Co(Phen)_2$/GCE, poly$(Cu(Bip)_2)$/GCE, and poly-$(Co(Phen)_2/Cu(Bip)_2)$/GCE was investigated by CV using 10 mM $[Fe(CN)_6]^{3-/4-}$ having 0.1 M KCl solution as a redox probe. Figure 4 demonstrates the CVs of 10 mM $[Fe(CN)_6]^{3-/4-}$ at the unmodified GCE, poly$(Co(Phen)_2$/GCE, poly$(Cu(Bip)_2)$/GCE, and poly$(Co(Phen)_2/Cu(Bip)_2)$/GCE at 100 mV/s. As shown in Figure 4, the poly$(Co(Phen)_2/Cu(Bip)_2)$/GCE shows exceedingly enhanced current response (I_p) and lower change in ΔEp as compared to the poly$(Co(Phen)_2$/GCE, poly$(Cu(Bip)_2)$/GCE, and unmodified GCE. The recorded I_p and ΔEp of GCE and poly$(Co(Phen)_2/Cu(Bip)_2)$/GCE were above 113- and 252-fold and 104.9 and 129 mV. These advances in the electrochemical behavior of poly(Co(Phen)2/Cu(Bip)2)/GCE might confirm the presence of a synergistic effect, speedy electron transference, and better effective surface area.[20,49]

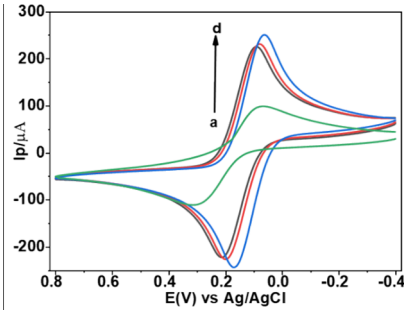

Figure 4. CV responses of 10.0 mM $[Fe(CN)_6]^{3-/4-}$ containing 0.1 M KCl (a) GCE, (b) poly$(Cu(Bip)_2)$/GCE, (c) poly$(Co(Phen)_2$/GCE, and (d) poly$(Co(Phen)_2/Cu(Bip)_2)$/GCE at a scan rate of 100 mV/s.

The effective surface areas of GCE, poly$(Cu(Bip)_2)$/GCE, poly$(Co(Phen)_2$/GCE, and poly$(Co(Phen)_2/Cu(Bip)_2)$/GCE were calculated using CV investigation by changing the scan rate in the range of 10 and 300 mV/s (Figure 5A–D). The areas of the bare GCE and all modified electrodes were revealed from the plot of the current response (Ip) against the square root of scan rate ($\nu^{1/2}$) using the Randles–Sevcik equation (eq 1).[50] The calculated areas of GCE, poly(Cu-$(Bip)_2)$/GCE, poly$(Co(Phen)_2$/GCE, and poly$(Co(Phen)_2$/$Cu(Bip)_2)$/GCE were 1.02, 2.87, 2.79, and 3.1 cm^2, respectively:

$$I_p = 2.69 \times 10^5 n^{3/2} A D^{1/2} C \nu^{1/2} \quad (1)$$

where n is the number of transferred electrons (=1), I_p is the peak current (μA), C is the concentration of $Fe(CN)_6^{3-/4-}$ (10 mM), ν scan rate (mV/s) and D is the diffusion coefficient of $Fe(CN)_6^{3-/4-}$ (7.7×10^{-6} cm^2/s).

3.3.3. Electrochemical Impedance Spectroscopy. The electrochemical behavior of GCE, poly$(Co(Phen)_2/Cu-(Bip)_2)$/GCE, poly$(Cu(Bip)_2)$/GCE, and poly$(Co(Phen)_2$/GCE was characterized by EIS, which is a profitable analytical technique to investigate the interfacial performance of electrodes.[51] The experimentation was achieved using 10 mM $Fe(CN)_6^{3-/4-}$ solution in the frequency range between 0.01 and 10,000 Hz. Figure 6 denotes the Nyquist plot of unmodified GCE (a), poly$(Co(Phen)_2/Cu(Bip)_2)$/GCE (b), poly$(Cu(Bip)_2)$/GCE (c), and poly$(Co(Phen)_2$/GCE (d). The linear and semicircle parts of the plot validate the presence of diffusion and charge transfer processes (R_{ct}), respectively, at the interface.[52] The R_{ct} quantities of the unmodified GCE, poly$(Cu(Bip)_2)$/GCE, poly$(Co(Phen)_2$/GCE, and poly$(Co-(Phen)_2/Cu(Bip)_2)$/GCE were 2,439, 57.18, 66.36, and 48.87 Ω respectively. As revealed in Figure 6, poly$(Co(Phen)_2/Cu(Bip)_2)$/GCE exhibits the lowest R_{ct} value, which is attributed to the existence of a quick charge transfer rate and is in covenant with the CV results. Moreover, the double layer capacitance (C_{dl}) and charge transfer rate (K_s) were measured based on eqs 2 and 3, respectively.

$$C_{dl} = \frac{1}{2\pi R_{ct} f_{max}} \quad (2)$$

$$K_s = \frac{RT}{n^2 F^2 C R_{ct}} \quad (3)$$

The values of the R_{ct}, solution resistance (R_s), frequency (f), C_{dl}, and K_s of the unmodified GCE, poly$(Cu(Bip)_2)$/GCE, poly$(Co(Phen)_2$/GCE, and poly$(Co(Phen)_2/Cu(Bip)_2)$/GCE are revealed in Table 1.

3.4. Electrochemical Oxidation of PCM and CQ. The simultaneous voltammetric responses of PCM and CQ at GCE and poly$(Co(phen)_2/Cu(Bip)_2)$/GCE were dealt with using CV measurement within the range 0 to 1.4 V at a scan rate of 100 mV/s. Figure 7 represents the CVs of 1 mM PCM and CQ in 0.1 M PBS at GCE and poly$(Co(phen)_2/Cu(Bip)_2)$/GCE that were conducted to evaluate the simultaneous electrochemical response of PCM and CQ. The poly$(Co(phen)_2/Cu(Bip)_2)$/GCE exhibits a more enhanced current response corresponding to the oxidation of CQ and PCM with respectable electrocatalytic behaviors. As compared to the GCE, the displayed peak current responses at poly(Co-$(phen)_2/Cu(Bip)_2)$/GCE were above 2.5- and 3.5-fold for PCM and CQ, respectively, which confirm the presence of an excellent effective surface area of poly$(Co(phen)_2/Cu(Bip)_2)$/GCE. Besides, about 112 and 98 mV shifts toward the more negative potential direction were observed, indicating the presence of an excellent electrocatalytic effect in $(Co(phen)_2/Cu(Bip)_2)$ bilayer polymeric films.

https://doi.org/10.1021/acsomega.4c08563
ACS Omega 2025, 10, 5601−5615

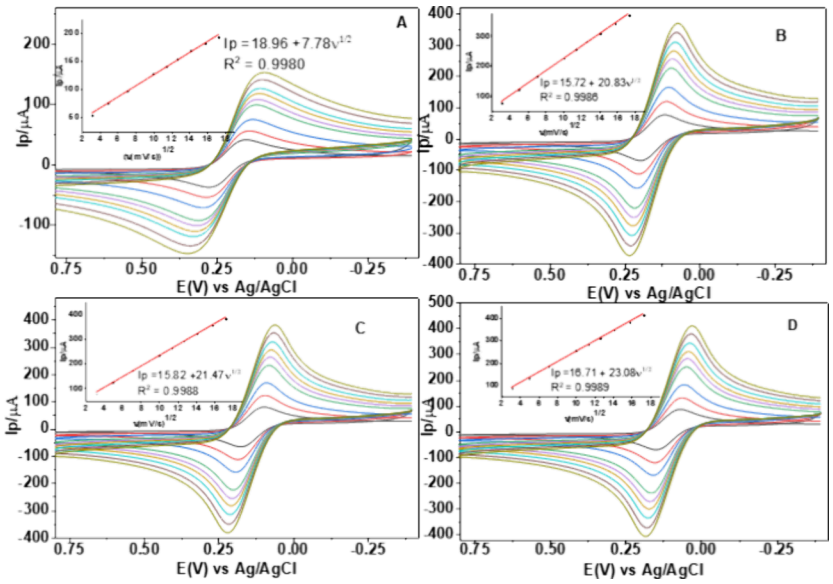

Figure 5. CVs of 10.0 mM $[Fe(CN)6]^{3-/4-}$ in KCl of 0.1 M (A) GCE, (B) poly$(Cu(Bip)_2)$/GCE, (C) poly$(Co(Phen)_2$/GCE, and (D) poly$(Co(Phen)_2/Cu(Bip)_2)$/GCE in the scan rate range between 10 and 300 mV/s (a−i: 10, 25, 50, 75, 100, 150, 200, 250, and 300, respectively). Inset: plot of I_p versus $v^{1/2}$.

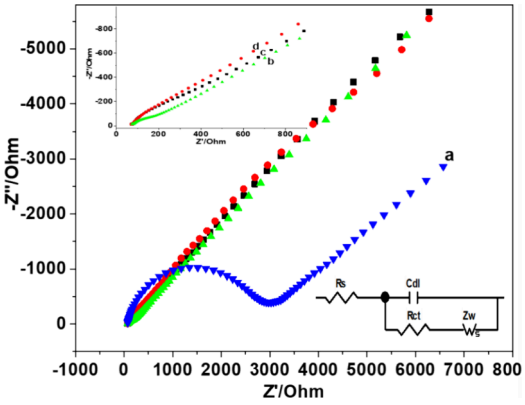

Figure 6. Nyquist plot of EIS found from (a) GCE, (b) poly$(Co(Phen)_2/Cu(Bip)_2)$/GCE (c) poly$(Cu(Bip)_2)$/GCE, and (d) poly$(Co(Phen)_2$/GCE toward 10.0 mM $[Fe(CN)6]^{3-/4-}$ in 0.1 M KCl in the frequency range between 0.01 and 10,000 Hz, amplitude: 0.01 V, and potential: 0.23 V. Inset: equivalent circuit model.

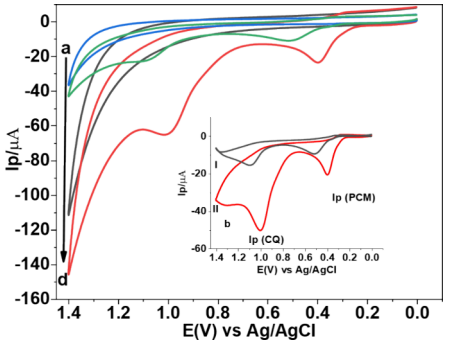

Figure 7. CVs of GCE (a and b) and poly$(Co(phen)_2/Cu(Bip)_2)$/GCE (c and d) in the absence (a and c) and presence of 1 mM PCM and CQ (b and d) in 0.1 M of PBS pH 7.0 at a scan rate of 100 mV/s (inset: blank corrected voltammograms of 1 mM PCM and CQ at GCE (I) and poly$(Co(phen)_2/Cu(Bip)_2)$/GCE (II)).

3.5. Influence of the Scan Rate on CQ and PCM Oxidation.

To examine the reaction mechanism, irreversibility, and kinetic parameters, the effect of the potential scan rate on the voltammetric responses of PCM and CQ was assessed by changing the scan rate parameter ranging between 25 and 300 mV/s through CV measurements. Figure 8 depicts the CVs of 0.5 mM PCM and CQ in PBS at pH 7 at poly$(Co(phen)_2/Cu(Bip)_2)$/GCE at various scan rates (between 25 and 300 mV/s). The results depict that the current signals of PCM and CQ were improved and shifted to the less negative potential with the increase in scan rates from 25 to 300 mV/s, proving the irreversibility of PCM and CQ oxidation at poly$(Co(phen)_2/Cu(Bip)_2)$/GCE. The correlation coefficient obtained from the plot of I_p against $v^{1/2}$ ($I_p/\mu A = -3.018 + 2.174\ v^{1/2}$, R^2=0.9970 and $I_p/\mu A = -8.2728 + 5.83\ v^{1/2}$, R^2 = 0.9936 (B)) was larger than the plot of I_p against v ($I_p/\mu A = 20.26 + 0.3036\ v$, R^2=0.9811 and $I_p/\mu A = 20.26 + 0.3036\ v$, R^2=0.9751 (C)), indicating that the oxidation of PCM and CQ at poly$(Co(phen)_2/Cu(Bip)_2)$/GCE is diffusion controlled. The slope (0.58 and 0.64) obtained from the plot of log I_p against log v ($I_p/\mu A = 0.1120 + 0.58\log v$, R^2=0.9980

Table 1. Calculated Value of Circuit Elements of EIS Examination at Different Electrodes

electrode type	R_s (Ω)	R_{ct} (Ω)	frequency (Hz)	K_s (cm^2)	C_{dl} (F)
GCE	65	2439	2.75	2.73×10^{-9}	2.37×10^{-5}
poly$(Cu(Bip)_2)$/GCE	65	66.36	1.94	1.00×10^{-7}	1.24×10^{-3}
poly$(Co(Phen)_2$/GCE	65	57.18	2.0	1.16×10^{-7}	1.39×10^{-3}
poly$(Co(Phen)_2/Cu(Bip)_2)$/GCE	65	48.87	2.08	1.36×10^{-7}	1.57×10^{-3}

https://doi.org/10.1021/acsomega.4c08563
ACS Omega 2025, 10, 5601−5615

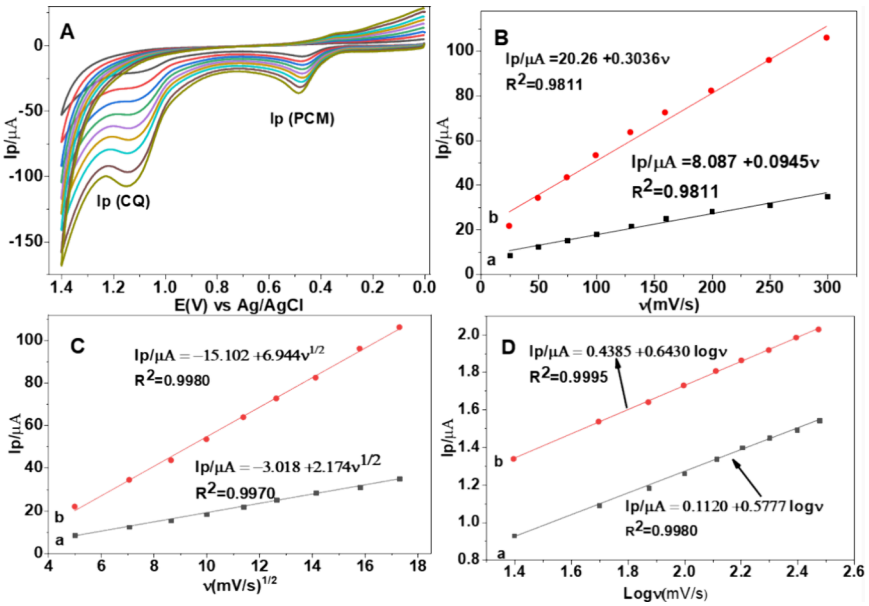

Figure 8. (A) CVs of 0.5 mM of PCM and CQ in PBS pH 7.0 at poly($(Phen)_2$/$Cu(Bip)_2$)/GCE of various scan rates (10 to 300: 10, 25, 50, 75, 100, 150, 200, 250, and 300 mV/s). (B) Plot of I_p versus ν. (C) Plot of I_p versus $\nu^{1/2}$. (D) Plot of the log I_p versus log ν.

and $I_p/\mu A$ = 0.4385 + 0.64log ν, R^2=0.9995 (D)), which is near 0.5 (the theoretical value of the diffusion process), also confirms that the oxidation of PCM and CQ is a diffusion-controlled process.

The transferred electrons (n) and the coefficient of electron transfer (α) values in PCM and CQ oxidation at poly-($(Phen)_2$/$Cu(Bip)_2$)/GCE were determined using eq 4.[50]

$$n = \frac{47.7}{a(E_p - E_{p1/2})} \quad (4)$$

The values of the maximum potential (E_p) and the half-peak potential ($E_{p1/2}$) for PCM oxidation were 443 and 389 mV, respectively. Similarly, the E_p and $E_{p1/2}$ values for the CQ oxidation reaction were 1128 and 1026 mV, respectively. The values of α for PCM and CQ oxidation at poly($(Phen)_2$/$Cu(Bip)_2$)/GCE were also determined based on eq 5.

$$E_p = E^0 + \frac{RT}{(1-\alpha)nF}\{0.780 + \ln(\frac{D_R^{1/2}}{K_0}) + \ln[\frac{(1-\alpha)nF\nu}{RT}]^{1/2}\} \quad (5)$$

The slope recorded from the plot of E_p against ln ν (E_p/V = 0.9398 + 0.0267ln ν, R^2 = 0.9981) is equal to $\frac{RT}{2n(1-\alpha)F}$(Figure 9). Based on eqs 4 and 5, the values of n and α for the electrochemical oxidation of PCM and CQ were calculated to be 2 and 1, and 0.62 and 0.42, respectively.

3.6. Influence of pH on PCM and CQ Oxidation. The influence of the pH variation on the oxidative current response and the peak potential of PCM and CQ at poly($Co(Phen)_2$/$Cu(Bip)_2$)/GCE was studied with CV by varying the pH of PBS from 4.5 to 9.0 at 100 mV/s. The CVs (in Figure 10A) show that the current signals of PCM and CQ were increased with the rise in pH from 4.5 to 6 and diminished beyond 6. Nonetheless, the current signal decayed progressively after pH 6, representing the existence of a strong Coulombic force of interaction between protonated PCM and CQ and the negatively charged $Co(Phen)_2$/$Cu(Bip)_2$ bilayer polymeric

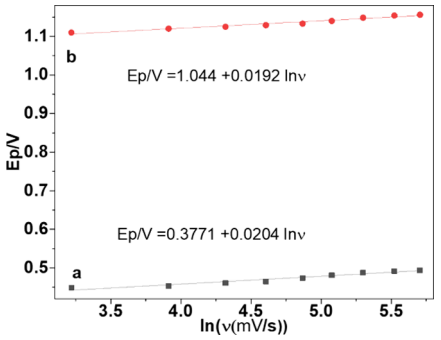

Figure 9. Plot of E_p versus ln ν of 0.5 mM PCM (a) and CQ (b) in 0.1 M PBS pH 7.0 at poly($Co(Phen)_2$/$Cu(Bip)_2$)/GCE at several scan rates ranging between 10 and 300 mV/s.

film.[53−55] The improvement in current response at the acidic pH (pH 6) might be related to the robust electrostatic interaction of the cationic PCM (p*K*a: 9.5)[55] and CQ (p*K*a: 8.4)[53,56] with negatively charged $Co(Phen)_2$/$Cu(Bip)_2$ bilayer polymeric film (p*K*a values of 2,2' bipyridine and 1, 10 phenanthroline were 4.47 and 4.93, respectively).[57,58] Thus, pH 6 was chosen as the optimum pH value for the succeeding simultaneous voltammetric investigations of PCM and CQ. Also, the peak potential of PCM and CQ was meaningfully shifted to a less negative direction when the pH value increased from 4.5 to 9 (Figure 10B), showing the proton participation in the simultaneous oxidation of PCM and CQ at poly($Co(Phen)_2$/$Cu(Bip)_2$)/GCE.[55,59] The perceived correlation between the E_p of PCM and CQ and the pH exhibits the regression equation of E_p/V = 1.483−0.0621 pH, R^2 = 0.9929 and Ep/V = 0.7592−0.0451 pH, R^2 = 0.9959, respectively (Figure 10C). A slope of 0.0621 and 0.0451 V/pH directs the participation of an equal number of electrons (ne^-) and protons (nH^+) in the electrode process. By bearing in mind the value of participating protons and electrons in the reaction process, the proposed reaction mechanism of PCM and CQ at poly($Co(Phen)_2$/$Cu(Bip)_2$)/GCE is pronounced in Scheme

https://doi.org/10.1021/acsomega.4c08563
ACS Omega 2025, 10, 5601−5615

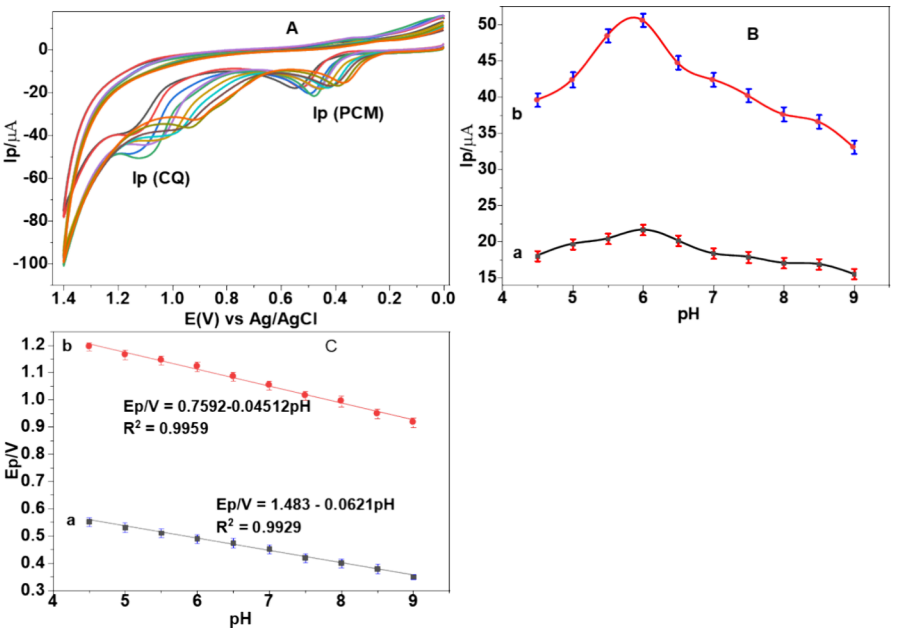

Figure 10. (A) CVs of 0.5 mM of PCM and CQ in 0.1 M of PBS of different pH values (a−g: 4.5, 5.5, 6, 6.5, 7, 7.5, 8, 8.5, and 9), (B) the plot of I_p of PCM and CQ versus pH, and C) the plot of E_p versus pH at poly(Co(Phen)$_2$/Cu(Bip)$_2$)/GCE at a scan rate of 100 mV/s.

2A,B, which is in agreement with the previous investigations.[3,54]

Scheme 2. Suggested Oxidation Mechanisms of PCM (A) and CQ (B) at Poly(Co(Phen)$_2$/Cu(Bip)$_2$)/GCE

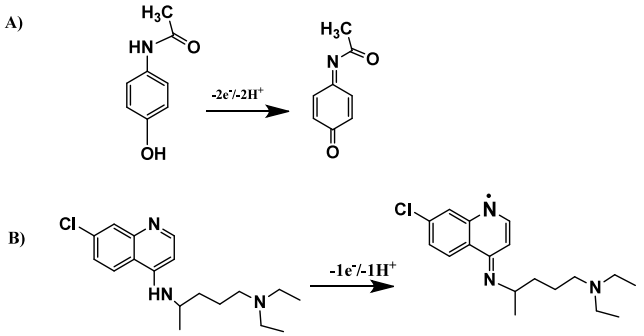

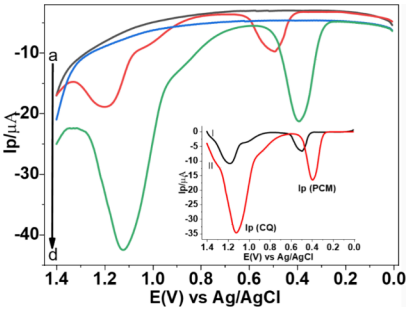

Figure 11. SWVs of bare GCE (a and c) and poly(Co(Phen)$_2$/Cu(Bip)$_2$)/GCE (b and d) in 0.1 M of PBS of pH 6.0 in the absence (a and b) and presence of 0.5 mM of PCM and CQ (c and d) at an increment of 4 mV, amplitude of 25 mV, frequency of 15 Hz, and scan rate of 100 mV/s. Inset: blank corrected SWVs of 0.5 mM CQ at GCE (I) and poly(Co(phen)$_2$/Cu(Bip)$_2$)/GCE (II).

3.7. Square Wave Voltammetric Study of CQ. Square wave voltammetry was preferred for the simultaneous quantitative determination of PCM and CQ in real samples owing to its rapid response and high sensitivity, low LOD, and minimized background current.[60] Figure 11 exhibits the SWVs of 0.5 mM PCM and CQ in PBS of pH 6 at poly(Co(Phen)$_2$/Cu(Bip)$_2$)/GCE. The observed current responses in GCE and poly(Co(Phen)$_2$/Cu(Bip)$_2$)/GCE were due to the oxidation of the amine and aminoquinoline moiety in the PCM and CQ molecules, respectively.[56,61] As depicted in Figure 11, the poly(Co(Phen)$_2$/Cu(Bip)$_2$)/GCE exhibits more enhanced oxidative peak current and excellent potential shift toward the less positive direction for PCM and CQ than the GCE. The resulting peak current, potential shift, and onset potential of poly(Co(Phen)$_2$/Cu(Bip)$_2$)/GCE for PCM and CQ were 17.2 μA, 110 mV, and 258 mV and 35.3 μA, 92 mV, and 916 mV, respectively. As compared to bare GCE, the current response enhancement of poly(Co(Phen)$_2$/Cu(Bip)$_2$)/GCE toward the oxidation of PCM and CQ was above 2.5- and 3.5-fold, respectively. Generally, the excellent potential shift, peak current enhancement, and lower onset potential of PCM and CQ oxidation might be due to the improved electrocatalytic property and superior effective surface area of the (Co-(Phen)$_2$/Cu(Bip)$_2$) bilayer film at the GCE surface.

3.8. Parameter Optimization. The step potential, pulse amplitude, and frequency were adjusted to investigate how the peak current of PCM and CQ oxidation depends on the SWV parameters and to provide the optimal experimental conditions for the simultaneous quantitative analysis of PCM and CQ in actual samples. At poly(Co(Phen)$_2$/Cu(Bip)$_2$)/GCE, the SWVs of 0.5 mM PCM and CQ at different step potentials (A), pulse amplitudes (B), and frequency (C) are shown in Figure S1 in 0.1 M PBS at pH 6. When the amplitude and frequency were fixed at 25 mV and 15 Hz, respectively, the peak current rose. When the step potential measurement was altered from 4 to 16 mV, a notable peak current increment was seen at 12 mV. The pulse amplitude effect was also studied in the 15−60 mV range by using the optimal step potential (12 mV) and keeping the frequency at 15 Hz. As the amplitude rose, the peak current rose from 15 to 60 mV, but the peak

https://doi.org/10.1021/acsomega.4c08563
ACS Omega 2025, 10, 5601−5615

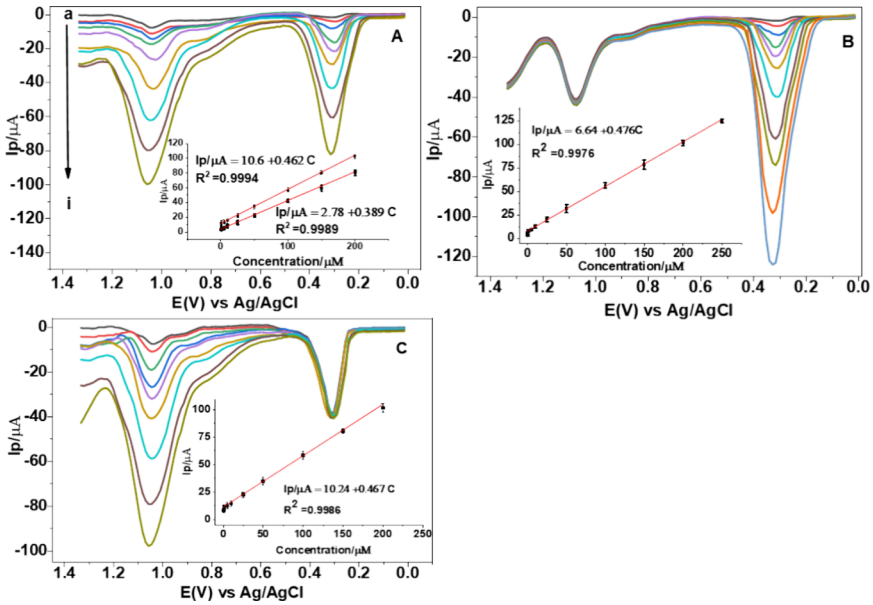

Figure 12. SWVs of different concentrations of (A) equimolar PCM and CQ (a−i: 0.5, 1, 5, 10, 25, 50, 100, 150, and 200 μM), (B) PCM (0.25, 0.5, 1, 5, 10, 25, 50, 100, 150, 200, and −250 μM), and (C) PCM (0.5, 1, 5, 10, 25, 50, 100, 150, and 200 μM) in PBS pH = 6.0 at poly(Co(Phen)$_2$/Cu(Bip)$_2$)/GCE at a scan rate of 100 mV/s, step potential of 12, amplitude of 45, and frequency of 40 Hz. Inset: plot of I_p versus concentration.

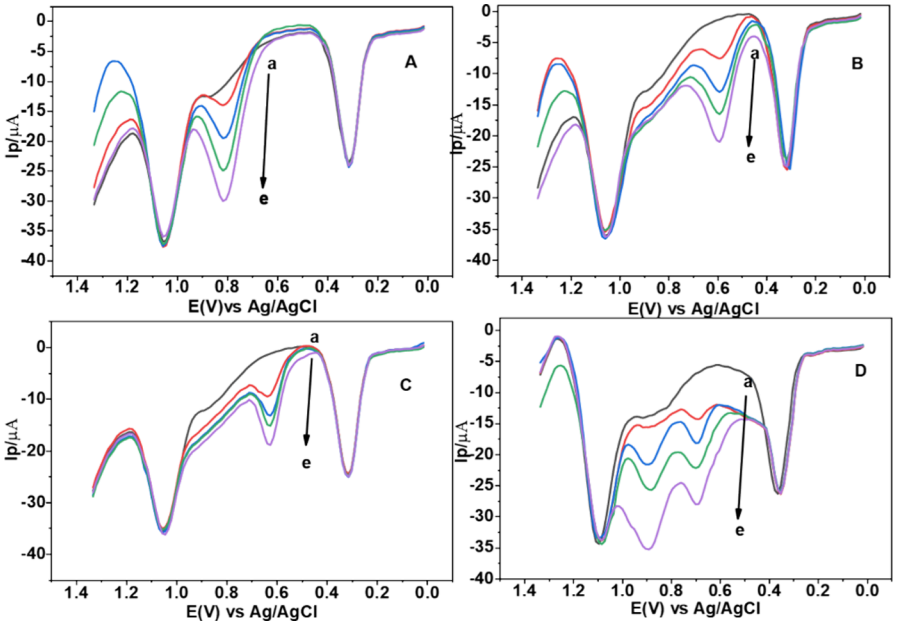

Figure 13. SWVs of 50.0 μM PCM and CQ in 0.1 M of PBS pH 6.0 at poly(Co(Phen)$_2$/Cu(Bip)$_2$)/GCE without (a) and with varied concentrations (25, 50, 75, and 100 μM (b−e)) of (A) SMX, (B) SBM, (C) Gua, and (D) ATS.

current barely ascended above 45 mV. Additionally, the impact of frequency was considered in the 10−50 Hz range by using the optimal step potential and pulse amplitudes of 12 and 45 mV, respectively. Both the PCM and CQ current signals dropped once the frequency was increased to 40 Hz. Since the peak's character was twisted and enlarged following the previously reported values, the ideal SWV parameters for the upcoming studies were determined to be a step potential of 12 mV, amplitude of 45 mV, and frequency of 40 Hz.

3.9. Calibration. The SWV measurement was carried out under optimized circumstances (pH: 6, step potential: 12 mV, pulse amplitude: 45 mV, and frequency: 40 Hz) to create the calibration curve for the simultaneous voltammetric assessment of PCM and CQ in actual samples. In 0.1 M PBS at pH 6, the current response of PCM and CQ was measured in the concentration range of 0.5 and 200 μM (Figure 12). As the concentrations of PCM and CQ increased, so did the current signals of PCM and CQ at poly(Co(Phen)$_2$/Cu(Bip)$_2$)/GCE. In addition, the current signal of PCM was examined in the concentration range between 0.25 and 250 μM at a fixed concentration (50 μM) of CQ. As can be perceived from Figure 12, the obtained current signals of PCM were increased linearly with concentration, while the value of the peak current of CQ was significantly constant (RSD = 2.9%). Correspond-

https://doi.org/10.1021/acsomega.4c08563
ACS Omega 2025, 10, 5601−5615

ingly, when the concentration of PCM was kept at 50 μM and CQ was varied in the range from 0.5 to 200 μM (Figure 12C), the current signal of CQ increased significantly with concentration, while the current response of PCM remained constant (RSD = 3.7%). The linear equations corresponding to the plot of I_p versus concentration of PCM and CQ were $I_p/\mu A = 2.78 + 0.389$ C, $R^2 = 0.9989$ and $I_p/\mu A = 10.6 + 0.462$ C, $R^2 = 0.9994$, respectively. The LOD (3δ/m) and LOQ ($10\ \delta$/m) values based on the sensitivity of the method (m, sensitivity = 0.389 and 0.462 $\mu A/\mu M$ for PCM and CQ, respectively) and the standard deviation of the background solution (δ) ($n = 10$) were 4.38×10^{-2} and 1.46×10^{-1} μM and 7.48×10^{-2} and 2.49×10^{-1} μM, respectively, for PCM and CQ.

3.10. Repeatability, Reproducibility, and Stability of Poly(Co(Phen)$_2$/Cu(Bip)$_2$)/GCE. Using SWV, the poly(Co(Phen)$_2$/Cu(Bip)$_2$)/GCE was tested for repeatability, reproducibility, and interday stability under optimal experimental situations (Figure S2). The poly(Co(Phen)$_2$/Cu(Bip)$_2$)/GCE repeatability was investigated using five SWV measurements of 0.5 mM PCM and CQ spaced 2 h apart throughout the day. The RSD of 3.1% ($n = 5$) for five duplicate measurements supports the good precision of the poly(Co(Phen)$_2$/Cu(Bip)$_2$)/GCE for PCM and CQ detection. Under comparable circumstances, the reproducibility of the poly(Co(Phen)$_2$/Cu(Bip)$_2$)/GCE was likewise examined using three distinct electrodes. The poly(Co(Phen)$_2$/Cu(Bip)$_2$)/GCE has admirable reproducibility against PCM and CQ oxidation, as shown by the RSD value (2.72% for $n = 3$). Six SWV investigations for 0.5 mM PCM and CQ at 2 day intervals and maintaining the poly(Co(Phen)$_2$/Cu(Bip)$_2$)/GCE in PBS at 4 °C in a fridge when not in utilization were additional methods used to evaluate the intraday stability of the established sensor. With $n = 6$, the electrode's RSD of 3.71% demonstrated its long-term stability for voltammetric PCM and CQ measurement.

3.11. Interference Study. The poly(Co(Phen)$_2$/Cu(Bip)$_2$)/GCE's ability to detect PCM and CQ simultaneously with potentially interfering compounds (such as sulfamethoxazole (SMX), salbutamol (SBM), guanine (Gua), and atorvastatin (ATS)) was investigated through a selectivity investigation conducted under optimal SWV conditions. To do the SWV measurement, the current response of 50 μM PCM and CQ with concentrations of 25, 50, 75, and 100 μM of each interference was recorded. Figure 13A–D shows the SWVs of 50 μM PCM and CQ both without and with various quantities (25 to 100 μM) of (A) SMX, (B) SBM, (C) Gua, and (D) ATS. The resulting current signals of 50 μM PCM and CQ obtained with and without each interference are summarized in Table S1. Furthermore, additional oxidation peaks emerged around 812, 588, 624, 690, and 892 mV toward the oxidation of PCM, SBM, Gua, and ATS, respectively, indicating the outstanding selectivity of the poly(Co(Phen)$_2$/Cu(Bip)$_2$)/GCE for PCM and CQ. The modification of the resultant current signals of PCM and CQ with various concentrations of each interference was in the 97.39–102.7% range.

3.12. Applications of Poly(Co(Phen)$_2$/Cu(Bip)$_2$)/GCE. The analytical application of poly(Co(Phen)$_2$/Cu(Bip)$_2$)/GCE was revealed under the optimized circumstances by sensing PCM and CQ in two pharmaceutical samples (ASKON, India, and EPHARM, Ethiopia). Figure 14 exhibits the SWVs of 25 and 50 μM PCM and CQ having 0.1 M PBS at the optimal pH for the ASKON and EPHARM brands. The recorded quantity of PCM and CQ was related to their brand value in the two medication formulations (Table 2). As

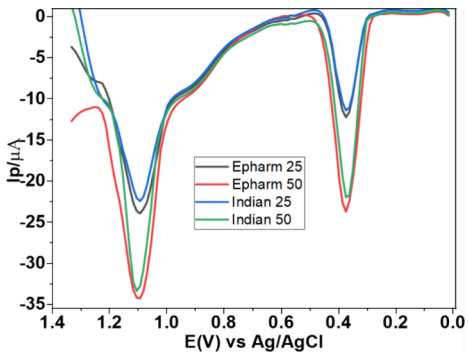

Figure 14. SWVs of 25.0 and 50.0 μM PCM and CQ in pH 6 PBS in two drug formulations (ASKON and EPHARM) at poly(Co(Phen)$_2$/Cu(Bip)$_2$)/GCE under the optimized experimental situations.

displayed in the table, the investigation of PCM and CQ in medication formulations revealed a mean recovery of more than 94.2%, confirming that the poly(Co(Phen)$_2$/Cu(Bip)$_2$)/GCE has respectable capability for the detection of PCM and CQ in drug samples. The recorded results are in agreement with the brand name value of the pharmaceuticals.

3.13. Recovery Analysis. *3.13.1. Pharmaceutical Samples.* To validate the established method for simultaneous SWV sensing of PCM and CQ in drug samples, the recovery investigation was conducted at poly(Co(Phen)$_2$/Cu(Bip)$_2$)/GCE. The analysis was performed by spiking 25 and 50 μM standard PCM and CQ solution into 50 μM EPHARM and ASKON drug samples. Figure 15 exhibits the SWVs of EPHARM (A) and ASKON (B) for 25 and 50 μM drug formulations without and with PCM and CQ standard solution. The spiked recovery responses of the EPHARM and ASKON drug samples are depicted in Table 3. As displayed in the table, the result of the spiked drug formulations was in the 98.9–106.1% range with RSD in the 1.95–3.86% range, showing that poly(Co(Phen)$_2$/Cu(Bip)$_2$)/GCE could be fruitfully employed for the simultaneous SWV determination of PCM and CQ in drug formulations.

3.13.2. Human Serum Sample. Likewise, the application of poly(Co(Phen)$_2$)/Cu(Bip)$_2$)/GCE for serum sample investigation was performed by spiking 0.5 mL of the serum sample with 25 and 50 μM PCM and CQ standard solution having 0.1 M PBS (pH = 6). Figure 16 exhibits the SWV of serum samples spiked with 25 and 50 μM PCM and CQ in pH 6 PBS at poly(Co(Phen)$_2$)/Cu(Bip)$_2$GCE. The presence of oxidative current signals (curve a) about 340 and 705 mV specifies the appearance of paracetamol and creatinine in serum samples.[62,63] The current response increases with spiked PCM and CQ, and the obtained spiked recoveries show the presence of PCM and CQ in the unspiked serum sample (curves a). As revealed in Table 4, spiked recoveries are in the 145.5–217.8% range with RSD below 3.9%, validating the prospective applicability of poly(Co(Phen)$_2$)/Cu(Bip)$_2$GCE for the simultaneous SWV sensing of PCM and CQ in serum samples.

3.13.3. Human Urine Sample. In a urine sample, the poly(Co(Phen)$_2$)/Cu(Bip)$_2$GCE's effectiveness for simultaneous SWV of PCM and CQ was also assessed. The SWVs of the unspiked and spiked (25 and 50 μM PCM and CQ) urine sample at poly(Co(Phen)$_2$)/Cu(Bip)$_2$GCE are shown in Figure 17. Uric acid and creatinine are present in the human urine sample, as indicated by the oxidative peaks i and iii (curve a) that were visible at 200 and 705 mV.[47,62] As shown

https://doi.org/10.1021/acsomega.4c08563
ACS Omega 2025, 10, 5601–5615

Table 2. Simultaneous SWV Determination of PCM and CQ in Pharmaceutical Samples

sample brand	label PCM (mg/tablet)	label CQ (mg/tablet)	expected PCM (μM)	expected CQ (μM)	detected PCM (μM)	detected CQ (μM)	PCM % recovery	CQ % recovery
EPHARM	500	250	25	25	24.8 ± 4.12	24.72 ± 3.41	99.2	98.88
			50	50	51.3 ± 3.62	49.03 ± 4.63	102.6	98.06
ASKON	500	250	25	25	23.96 ± 3.22	23.75 ± 2.93	94.92	94.2
			50	50	49.87 ± 3.90	47.80 ± 3.87	99.74	95.6

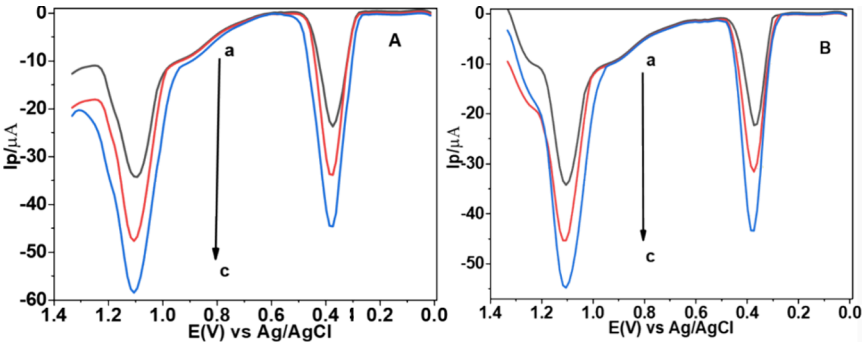

Figure 15. Blank corrected SWVs of EPHARM (A) and ASKON (B) drug formulations unspiked and spiked with 25 and 50 μM PCM and CQ (curve a to c) at poly(Co(Phen)$_2$)/Cu(Bip)$_2$)/GCE at a scan rate 100 mV/s, step potential of 12, amplitude of 45, and frequency of 40 Hz.

Table 3. Recovery Results of Spiked PCM and CQ Solutions in Drug Formulations

tablet brand	added	initial PCM (μM)	initial CQ(μM)	detected PCM (μM)	detected CQ (μM)	% recovery PCM	% recovery CQ
EPHARM	0	51.3	49.0 ± 2.13				
	25	51.3	49.0 ± 2.13	77.17 ± 3.11	75.5 ± 3.85	103.5	105.9
	50	51.3	49.0 ± 2.13	102.1 ± 2.91	102.1 ± 3.17	101.6	106.1
ASKON	0	49.87	47.8 ± 4.14				
	25	49.87	47.8 ± 4.14	74.60 ± 3.38	73.3 ± 2.96	98.9	102.1
	50	49.87	47.8 ± 4.14	100.3 ± 3.14	99.5 ± 1.95	100.8	103.4

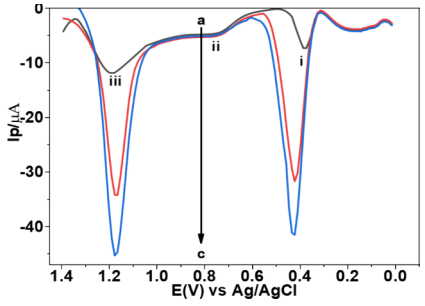

Figure 16. SWVs of unspiked and spiked (25 and 50 μM of PCM and CQ) serum samples (curve a to c) at poly(Co(Phen)$_2$)/Cu-(Bip)$_2$GCE at a scan rate 100 mV/s, step potential of 12 mV, amplitude of 45, and frequency of 40 Hz.

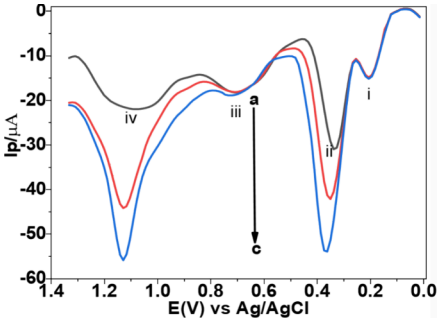

Figure 17. SWVs of unspiked and spiked (25 and 50 μM of PCM and CQ) urine samples (a to c) at poly(Co(Phen)$_2$)/Cu(Bip)$_2$GCE at a scan rate of 100 mV/s, step potential of 12 mV, amplitude of 45, and frequency of 40 Hz.

in the oxidative peak current (ii and iv) exhibited around the oxidative peak potential of PCM and CQ (curve a), the obtained data from the spiked recovery analysis of PCM and CQ confirm the presence of PCM and CQ in the unspiked urine sample. Table 5 demonstrates the analytical application of poly(Co(Phen)$_2$)/Cu(Bip)$_2$GCE for SWV detection of PCM and CQ in human urine samples, with spiking recoveries ranging between 113.8 and 192% and an RSD < 4.2%.

Table 4. Spiked Recoveries PCM and CQ in Human Serum

sample	added	current response (μA)		found (μM)		RSD %		recovery %	
		PCM	CQ	PCM	CQ	PCM	CQ	PCM	CQ
serum	0	7.3	12.0	11.92	3.03				
	25	28.6	34.3	66.38	51.30	4.17	1.6	217.8	193.1
	50	39.1	45.6	93.37	75.76	3.05	3.9	162.9	145.5

https://doi.org/10.1021/acsomega.4c08563
ACS Omega 2025, 10, 5601−5615

Table 5. Spiked Recoveries PCM and CQ in a Human Urine Sample

		current response (μA)		found (μM)		RSD %		recovery %	
sample	added	PCM	CQ	PCM	CQ	PCM	CQ	PCM	CQ
serum	0	31.0	22.1	72.5	24.9				
	25	43.4	44.3	104.4	72.9	2.37	4.2	127.6	192
	50	53.1	55.4	129.4	97.0	3.5	3.8	113.8	144.2

4. CONCLUSIONS

To determine PCM and CQ simultaneously using voltammetry, poly(Co(Phen)$_2$/Cu(Bip)$_2$)/GCE was successfully introduced in this work. This was based on the successive electropolymerization of [Co(Phen)$_2$(H$_2$O)$_2$]l$_2$·2H$_2$O and [Cu(Bip)$_2$Cl]I at GCE. The manufacture of electroactive bilayer (poly(Co(Phen)$_2$/Cu(Bip)$_2$)) polymeric films at GCE is proven by the FTIR, CV, and EIS characterization results. Compared to GCE, poly(Co(Phen)$_2$/GCE, and poly(Cu(Bip)$_2$)/GCE, the simultaneous SWV result of poly(Co(Phen)$_2$/Cu(Bip)$_2$)/GCE to PCM and CQ oxidation was greater. For simultaneous SWV examination of PCM and CQ in a wide linear range (0.5−200 μM) with low LOD value (4.38×10^{-2} and 7.48×10^{-2} μM, respectively), poly(Co(Phen)$_2$/Cu(Bip)$_2$)/GCE shows high sensitivity.

Poly(Co(Phen)$_2$/Cu(Bip)$_2$)/GCE's selectivity for PCM and CQ sensing was investigated with atorvastatin, guanine, salbutamol, and sulfamethoxazole. With impressive recovery rates, the established sensor was successfully used for the simultaneous SWV measurement of PCM and CQ in pharmaceutical, serum, and urine samples. This suggests that the Poly(Co(Phen)$_2$/Cu(Bip)$_2$)/GCE for the simultaneous electrochemical sensing of PCM and CQ in real samples is promising.

■ ASSOCIATED CONTENT

Supporting Information

The Supporting Information is available free of charge at https://pubs.acs.org/doi/10.1021/acsomega.4c08563.

Additional evidence for the present work: Figure S1 describes the optimization of SWV parameters, including the step potential, amplitude, and frequency; Figure S2 designates the repeatability, reproducibility, and stability of the developed sensor for simultaneous voltammetric determination of paracetamol and chloroquine under the optimized experimental conditions; and Table S1 also summarizes the selectivity of the established bilayered film-modified glassy carbon electrode and the effect of potentially interfering substances for simultaneous voltammetric determination of paracetamol and chloroquine (PDF)

■ AUTHOR INFORMATION

Corresponding Authors

Mulu Gashu − *Department of Chemistry, College of Science, Bahir Dar University, Bahir Dar 1000, Ethiopia; Department of Chemistry, College of Natural and Computational Sciences, Mekdela Amba University, Mekane Selam 1000, Ethiopia;* orcid.org/0009-0004-5244-2713; Email: mulugashu16@gmail.com

Belete Asefa Aragaw − *Department of Chemistry, College of Science, Bahir Dar University, Bahir Dar 1000, Ethiopia;* orcid.org/0000-0003-4801-7197; Email: beliyeeed@gmail.com

Molla Tefera − *Department of Chemistry, University of Gondar, Gondar 1000, Ethiopia;* orcid.org/0000-0003-4469-5388; Email: mollatef2001@gmail.com

Author

Atakilt Abebe − *Department of Chemistry, College of Science, Bahir Dar University, Bahir Dar 1000, Ethiopia;* orcid.org/0000-0002-5496-664X

Complete contact information is available at: https://pubs.acs.org/10.1021/acsomega.4c08563

Notes

The authors declare no competing financial interest.

■ ACKNOWLEDGMENTS

The authors acknowledge the Ethiopian Food and Drug Administration Authority (EFDA) for providing standards for chloroquine phosphate and paracetamole. The Bahir Dar University's College of Science is also acknowledged for the access to laboratory resources. Moreover, SIDA (the Swedish International Development Cooperation Agency) through the ISP (International Science Program, Uppsala University) is acknowledged for financial support.

■ REFERENCES

(1) Bertolini, A.; Ferrari, A.; Ottani, A.; Guerzoni, S.; Tacchi, R.; Leone, S. *Paracetamol: New Vistas of an Old Drug.* **2006**, *12* (3−4), 250−275.

(2) Jefferies, S.; Saxena, M.; Young, P. Paracetamol in critical illness: a review. *Critical Care and Resuscitation* **2012**, *14* (1), 74−80.

(3) Martin Santos, A.; Wong, A.; Araújo Almeida, A.; Fatibello-Filho, O. Simultaneous determination of paracetamol and ciprofloxacin in biological fluid samples using a glassy carbon electrode modified with graphene oxide and nickel oxide nanoparticles. *Talanta* **2017**, *174*, 610−618.

(4) Beck, D. H.; Schenk, M. R.; Hagemann, K.; Doepfmer, U. R.; Kox, W. J. The Pharmacokinetics and Analgesic Efficacy of Larger Dose Rectal Acetaminophen (40 mg/kg) in Adults: A Double-Blinded, Randomized Study. *Anesth. Analg.* **2000**, *90* (2), 431.

(5) Jaeschke, H.; Williams, C. D.; Ramachandran, A.; Bajt, M. L. Acetaminophen hepatotoxicity and repair: the role of sterile inflammation and innate immunity. *Liver International* **2012**, *32* (1), 8−20.

(6) Soliman, M. M.; Nassan, M. A.; Ismail, T. A. Immunohistochemical and molecular study on the protective effect of curcumin against hepatic toxicity induced by paracetamol in Wistar rats. *BMC Complementary Altern. Med.* **2014**, *14* (1), 457.

(7) Maksymowych, W.; Russell, A. S. Antimalarials in rheumatology: Efficacy and safety. *Seminars in Arthritis and Rheumatism* **1987**, *16* (3), 206−221.

(8) Thompson, P. *Antimalarial agents: chemistry and pharmacology.* Elsevier: 2012; Vol. *12*.

(9) M, M.; Stimpfl, T.; Malzer, R.; Mortinger, H.; Binder, R.; Vycudilik, W.; Berzlanovich, A.; Bauer, G.; Laggner, A. N. Suicidal chloroquine poisoning: clinical course, autopsy findings, and chemical analysis. *J. Forensic Sci.* **1996**, *41* (6), 1077−1079.

(10) Srinivasa, A.; Tosounidou, S.; Gordon, C. Increased Incidence of Gastrointestinal Side Effects in Patients Taking Hydroxychloroquine: A Brand-related Issue? *J. Rheumatol.* **2017**, *44* (3), 398.1.
(11) González-Hein, G.; Cordero, N.; García, P.; Figueroa, G. Molecular analysis of fluoroquinolones and macrolides resistance in Campylobacter jejuni isolates from humans, bovine and chicken meat. *Rev. Chilena Infectol* **2013**, *30* (2), 135−139.
(12) Baird, J. K. Chloroquine Resistance in Plasmodium vivax. *Antimicrob. Agents Chemother.* **2004**, *48* (11), 4075−4083.
(13) White, N. J. Cardiotoxicity of antimalarial drugs. *Lancet Infectious Diseases* **2007**, *7* (8), 549−558.
(14) Kingsley, M. P.; Kalambate, P. K.; Srivastava, A. K. Simultaneous determination of ciprofloxacin and paracetamol by adsorptive stripping voltammetry using copper zinc ferrite nanoparticles modified carbon paste electrode. *RSC Adv.* **2016**, *6* (18), 15101−15111.
(15) Toama, M. A.; El Fatatry, H. M.; El Falaha, B. In Vitro Studies on Drug−Antibiotic Interactions I: Analgesics, Antipyretics, Antimalarials, and Tranquilizers. *J. Pharm. Sci.* **1978**, *67* (1), 23−26.
(16) Green, M. D.; Nettey, H.; Rojas, O. V.; Pamanivong, C.; Khounsaknalath, L.; Ortiz, M. G.; Newton, P. N.; Fernández, F. M.; Vongsack, L.; Manolin, O. Use of refractometry and colorimetry as field methods to rapidly assess antimalarial drug quality. *J. Pharm. Biomed. Anal.* **2007**, *43* (1), 105−110.
(17) Miranda, T. A.; Silva, P. H.; Pianetti, G. A.; César, I. C. Simultaneous quantitation of chloroquine and primaquine by UPLC-DAD and comparison with a HPLC-DAD method. *Malaria J.* **2015**, *14* (1), 29.
(18) Hassan, S. A.; Ibrahim, N.; Elzanfaly, E. S.; El Gendy, A. E. Analytical quality by design approach for the control of potentially counterfeit chloroquine with some NSAIDS using HPLC with fluorescence detection in pharmaceutical preparation and breast milk. *Acta Chromatographica AChrom* **2021**, *33* (3), 234−244.
(19) Zhang, H.; Zhao, J.; Liu, H.; Wang, H.; Liu, R.; Liu, J. J. I. J. E. S. Application of poly (3-methylthiophene) modified glassy carbon electrode as riboflavin sensor. *Int. J. Electrochem. Sci.* **2010**, *5*, 295−301.
(20) Ghasemi, E.; Alimardani, E.; Shams, E.; Koohmareh, G. A. Modification of glassy carbon electrode with iron-terpyridine complex and iron-terpyridine complex covalently bonded to ordered mesoporous carbon substrate: Preparation, electrochemistry and application to H2O2 determination. *J. Electroanal. Chem.* **2017**, *789*, 92−99.
(21) Ribeiro, G. H.; Vilarinho, L. M.; Ramos, T. d. S.; Bogado, A. L.; Dinelli, L. R. Electrochemical behavior of hydroquinone and catechol at glassy carbon electrode modified by electropolymerization of tetraruthenated oxovanadium porphyrin. *Electrochim. Acta* **2015**, *176*, 394−401.
(22) Essa, W. A.; Beltagi, A. M.; Hathoot, A. A.; Azzem, M. A. A Sensitive Voltammetric Sensor for Improved Simultaneous Determination of Moxifloxacin Hydrochloride and Paracetamol. *J. Electrochem. Soc.* **2020**, *167* (16), No. 167509.
(23) Švorc, Ľ.; Sochr, J.; Tomčík, P.; Rievaj, M.; Bustin, D. Simultaneous determination of paracetamol and penicillin V by square-wave voltammetry at a bare boron-doped diamond electrode. *Electrochim. Acta* **2012**, *68*, 227−234.
(24) Lisboa, T. P.; de Faria, L. V.; de Oliveira, W. B. V.; Oliveira, R. S.; de Souza, C. C.; Matos, M. A. C.; Dornellas, R. M.; Matos, R. C. Simultaneous monitoring of amoxicillin and paracetamol in synthetic biological fluids using a 3D printed disposable electrode with a lab-made conductive filament. *Anal. Bioanal. Chem.* **2024**, *416* (1), 215−226.
(25) Nataraj, N.; Chen, S.-M.; Krishnan, S. K. Strontium vanadate-supported graphitic carbon nitride nanocomposite for simultaneous voltammetric determination of acetaminophen and levofloxacin in complex biological samples. *Environmental Science: Nano* **2022**, *9* (10), 3927−3942.
(26) Khoobi, A.; Ghoreishi, S. M.; Behpour, M.; Shaterian, M.; Salavati-Niasari, M. Design and evaluation of a highly sensitive nanostructure-based surface modification of glassy carbon electrode for electrochemical studies of hydroxychloroquine in the presence of acetaminophen. *Colloids Surf., B* **2014**, *123*, 648−656.
(27) Oiye, É. N.; Ribeiro, M. F. M.; Katayama, J. M. T.; Tadini, M. C.; Balbino, M. A.; Eleotério, I. C.; Magalhães, J.; Castro, A. S.; Silva, R. S. M.; da Cruz Júnior, J. W.; Dockal, E. R.; de Oliveira, M. F. Electrochemical sensors containing Schiff bases and their transition metal complexes to detect analytes of forensic, pharmaceutical and environmental interest. A review. *Crit. Rev. Anal. Chem.* **2019**, *49* (6), 488−509.
(28) Song, S.; Xue, Y.; Feng, L.; Elbatal, H.; Wang, P.; Moorefield, C. N.; Newkome, G. R.; Dai, L. Reversible Self-Assembly of Terpyridine-Functionalized Graphene Oxide for Energy Conversion. *Angew. Chem., Int. Ed.* **2014**, *53* (5), 1415−1419.
(29) Schott, M.; Szczerba, W.; Kurth, D. G. Detailed Study of Layer-by-Layer Self-Assembled and Dip-Coated Electrochromic Thin Films Based on Metallo-Supramolecular Polymers. *Langmuir* **2014**, *30* (35), 10721−10727.
(30) Liu, B.; Huang, H.-X.; Zhang, C.-F.; Chen, M.; Qian, D.-J. Monolayers, Langmuir−Blodgett films of bimetallic coordination polymers of 4′-(4-pyridyl)-2,2′:6′,2″-terpyridine. *Thin Solid Films* **2008**, *516* (8), 2144−2150.
(31) Ramos Sende, J. A.; Arana, C. R.; Hernandez, L.; Potts, K. T.; Keshevarz-K, M.; Abruna, H. D. Electrocatalysis of CO2 Reduction in Aqueous Media at Electrodes Modified with Electropolymerized Films of Vinylterpyridine Complexes of Transition Metals. *Inorg. Chem.* **1995**, *34* (12), 3339−3348.
(32) Buczkowska, M. K.*Synthesis, characterization, antitumor and antimicrobial activities of heterocyclic transition metal complexes*. 2011.
(33) Cruz-Navarro, J. A.; Hernández-García, F.; Mendoza-Huizar, L. H.; Salazar-Pereda, V.; Cobos-Murcia, J. Á.; Colorado-Peralta, R.; Álvarez-Romero, G. A. Recent Advances in the Use of Transition-Metal Porphyrin and Phthalocyanine Complexes as Electro-Catalyst Materials on Modified Electrodes for Electroanalytical Sensing Applications. *Solids* **2021**, *2*, 212−231.
(34) Kassa, A.; Abebe, A.; Amare, M. Synthesis, characterization, and electropolymerization of a novel Cu(II) complex based on 1,10-phenanthroline for electrochemical determination of amoxicillin in pharmaceutical tablet formulations. *Electrochim. Acta* **2021**, *384*, No. 138402.
(35) Ramdass, A.; Sathish, V.; Babu, E.; Velayudham, M.; Thanasekaran, P.; Rajagopal, S. Recent developments on optical and electrochemical sensing of copper(II) ion based on transition metal complexes. *Coord. Chem. Rev.* **2017**, *343*, 278−307.
(36) Oiye, É. N.; Ribeiro, M. F. M.; Katayama, J. M. T.; Tadini, M. C.; Balbino, M. A.; Eleotério, I. C.; Magalhães, J.; Castro, A. S.; Silva, R. S. M.; da Cruz Júnior, J. W.; Dockal, E. R.; de Oliveira, M. F. Electrochemical Sensors Containing Schiff Bases and their Transition Metal Complexes to Detect Analytes of Forensic, Pharmaceutical and Environmental Interest. A Review. *Critical Reviews in Analytical Chemistry* **2019**, *49* (6), 488−509.
(37) Metto, M.; Tesfaye, A.; Atlabachew, M.; Abebe, A. Synthesis, characterization, and electrochemical application of novel poly-(Cu2P4BCl4) based glassy carbon electrodes for determination of sulfamethoxazole in pharmaceutical serum and urine samples and Cow's milk. *Microchemical Journal* **2024**, *201*, No. 110627.
(38) McCreery, R. L. Advanced Carbon Electrode Materials for Molecular Electrochemistry. *Chem. Rev.* **2008**, *108* (7), 2646−2687.
(39) Hoa, D. T. N.; Tu, N. T. T.; Son, L. V. T.; Son, L. V. T.; Toan, T. T. T.; Thong, P. L. M.; Nhiem, D. N.; Lieu, P. K.; Khieu, D. Q.; Le, T. S. Electrochemical Determination of Diclofenac by Using ZIF-67/g-C3N4Modified Electrode. *Adsorpt. Sci. Technol.* **2021**, *2021*, No. 7896286.
(40) He, Y.; Zhong, C.; Zhou, Y.; Zhang, H. Synthesis and luminescent properties of novel Cu (II), Zn (II) polymeric complexes based on 1,10-phenanthroline and biphenyl groups. *Journal of Chemical Sciences* **2009**, *121* (4), 407−412.
(41) Senthil Kumar, R.; Sasikala, K.; Arunachalam, S. DNA interaction of some polymer−copper(II) complexes containing 2,2′-

https://doi.org/10.1021/acsomega.4c08563
ACS Omega 2025, 10, 5601−5615

bipyridyl ligand and their antimicrobial activities. *Journal of Inorganic Biochemistry* **2008**, *102* (2), 234−241.
(42) Marcon, G.; Carotti, S.; Coronnello, M.; Messori, L.; Mini, E.; Orioli, P.; Mazzei, T.; Cinellu, M. A.; Minghetti, G. Gold(III) Complexes with Bipyridyl Ligands: Solution Chemistry, Cytotoxicity, and DNA Binding Properties. *J. Med. Chem.* **2002**, *45* (8), 1672−1677.
(43) Kuntoji, G.; Kousar, N.; Gaddimath, S.; Koodlur Sannegowda, L. Macromolecule−Nanoparticle-Based Hybrid Materials for Biosensor Applications. *Biosensors* **2024**, 277.
(44) Palanna, M.; Mohammed, I.; Aralekallu, S.; Nemakal, M.; Sannegowda, L. K. Simultaneous detection of paracetamol and 4-aminophenol at nanomolar levels using biocompatible cysteine-substituted phthalocyanine. *New J. Chem.* **2020**, *44* (4), 1294−1306.
(45) Rasheed, T.; Rizwan, K. Metal-organic frameworks based hybrid nanocomposites as state-of−the-art analytical tools for electrochemical sensing applications. *Biosens. Bioelectron.* **2022**, *199*, No. 113867.
(46) Gashu, M.; Aragaw, B. A.; Tefera, M.; Abebe, A. Poly(bis(2,2′-bipyridine) hydroxy Copper(II) iodide modified glassy carbon electrode for electrochemical determination of chloroquine in pharmaceuticals and biological samples. *Sensing and Bio-Sensing Research* **2023**, *42*, No. 100598.
(47) Gashu, M.; Aragaw, B. A.; Tefera, M.; Abebe, A. Cobalt(II) bis-(1,10-phenanthroline) complex electropolymerized glassy carbon electrode and its electrocatalytic sensing of diclofenac in pharmaceuticals and biological samples. *Colloids Surf., A* **2024**, *693*, No. 133974.
(48) Liu, W.; Huang, W.; Pink, M.; Lee, D. Layer-by-Layer Synthesis of Metal-Containing Conducting Polymers: Caged Metal Centers for Interlayer Charge Transport. *J. Am. Chem. Soc.* **2010**, *132* (34), 11844−11846.
(49) Deepa, S.; Swamy, B. E. K.; Pai, K. V. A surfactant SDS modified carbon paste electrode as an enhanced and effective electrochemical sensor for the determination of doxorubicin and dacarbazine its applications: A voltammetric study. *J. Electroanal. Chem.* **2020**, *879*, No. 114748.
(50) Bard, A. J.; Faulkner, L. R. *Student Solutions Manual to accompany Electrochemical Methods: Fundamentals and Applicaitons, 2e*. John Wiley & Sons: 2002.
(51) Yaman, Y. T.; Abaci, S. Sensitive Adsorptive Voltammetric Method for Determination of Bisphenol A by Gold Nanoparticle/Polyvinylpyrrolidone-Modified Pencil Graphite Electrode. *Sensors* **2016**, 756.
(52) Maroneze, C. M.; Rahim, A.; Fattori, N.; da Costa, L. P.; Sigoli, F. A.; Mazali, I. O.; Custodio, R.; Gushikem, Y. Electroactive Properties of 1-propyl-3-methylimidazolium Ionic Liquid Covalently Bonded on Mesoporous Silica Surface: Development of an Electrochemical Sensor Probed for NADH, Dopamine and Uric Acid Detection. *Electrochim. Acta* **2014**, *123*, 435−440.
(53) Yi, X.-H.; Ji, H.; Wang, C.-C.; Li, Y.; Li, Y.-H.; Zhao, C.; Wang, A.; Fu, H.; Wang, P.; Zhao, X.; Liu, W. Photocatalysis-activated SR-AOP over PDINH/MIL-88A(Fe) composites for boosted chloroquine phosphate degradation: Performance, mechanism, pathway and DFT calculations. *Applied Catalysis B: Environmental* **2021**, *293*, No. 120229.
(54) Oliveira, G. G.; Azzi, D. C.; Silva, T. A.; Oliveira, P. R.; Fatibello-Filho, O.; Janegitz, B. C. Sensitive Voltammetric Detection of Chloroquine Drug by Applying a Boron-Doped Diamond Electrode *C. J. Carbon Res.* **2020**.
(55) Fernandez, C.; Heger, Z.; Kizek, R.; Ramakrishnappa, T.; Boruń, A.; Faisal, N. H. Pharmaceutical Electrochemistry: the Electrochemical Oxidation of Paracetamol and Its Voltammetric Sensing in Biological Samples Based on Screen Printed Graphene Electrodes. *Int. J. Electrochem. Sci.* **2015**, *10* (9), 7440−7452.
(56) Srivastava, M.; Tiwari, P.; Mall, V. K.; Srivastava, S. K.; Prakash, R. Voltammetric determination of the antimalarial drug chloroquine using a glassy carbon electrode modified with reduced graphene oxide on WS2 quantum dots. *Microchimica Acta* **2019**, *186* (7), 415.
(57) Fan, J.; Wang, J.; Ye, C. Acid−base dissociation constants of 2,2′-bipyridyl in mixed protic solvents. *Talanta* **1998**, *46* (6), 1285−1292.
(58) Doe, H.; Yoshioka, K.; Kitagawa, T. Voltammetric study of protonated 1,10-phenanthroline cation transfer across the water/nitrobenzene interface. *J. Electroanal. Chem.* **1992**, *324* (1), 69−78.
(59) Gashu, M.; Aragaw, B.; Tefera, M. Voltammetric Determination of Oxytetracycline in Milk and Pharmaceuticals samples using Polyurea Modified Glassy Carbon Electrode. *Journal of Food Composition and Analysis* **2023**, *117*, No. 105128.
(60) Aoki, K.; Osteryoung, J. Square wave voltammetry in a thin-layer cell. *Journal of Electroanalytical Chemistry and Interfacial Electrochemistry* **1988**, *240* (1), 45−51.
(61) Remziye Güzel; Ekşi, H.; Dinç, E.; Solak, A. O. New Voltammetric Approach to the Quantitation of Paracetamol in Tablets and Syrup using Chemometric Optimization Technique. *J. Anal. Chem.* **2019**, *74* (3), 296−305.
(62) Randviir, E. P.; Kampouris, D. K.; Banks, C. E. An improved electrochemical creatinine detection method via a Jaffe-based procedure. *Analyst* **2013**, *138* (21), 6565−72.
(63) Sripirom, J.; Sim, W. C.; Khunkaewla, P.; Suginta, W.; Schulte, A. Simple and Economical Analytical Voltammetry in 15 μL Volumes: Paracetamol Voltammetry in Blood Serum as a Working Example. *Anal. Chem.* **2018**, *90* (17), 10105−10110.

https://doi.org/10.1021/acsomega.4c08563
ACS Omega 2025, 10, 5601−5615